EFFECTS OF RESIDUAL STRESSES AND INITIAL IMPERFECTIONS ON EARTHQUAKE RESPONSE OF STEEL MOMENT FRAMES

BY

KAPIL MATHUR

THESIS

Submitted in partial fulfillment of the requirements
for the degree of Master of Science in Civil Engineering
in the Graduate College of the
University of Illinois at Urbana-Champaign, 2011

Urbana, Illinois

Adviser:

Assistant Professor Larry A. Fahnestock

ABSTRACT

The 2010 AISC *Specification* establishes the Direct Analysis Method (DM) as the standard stability analysis and design procedure. Although the DM has important benefits over conventional stability design methods, the interface between the DM, the AISC *Seismic Provisions* and the seismic design requirements in *ASCE-7* is not fully established. Since the DM, which was developed for design scenarios that do not contain seismic loading, includes the effects of initial geometric imperfections and inelastic behavior compounded by residual stresses, it is critical to explore the impact of these parameters on the seismic behavior of typical steel buildings before the DM is required for seismic design.

To examine these issues, a series of steel special moment-resisting frame models were subjected to monotonic pushover, cyclic pushover and response history analyses. The observed behavior was used to draw comparisons between systems with and without residual stresses and initial imperfections. Cyclic strength degradation at beam-to-column connections was also considered to examine the potential interaction it may have with the other parameters. Whereas the well-known impact of strength degradation on cyclic stability was noted, residual stresses and initial imperfections did not have any appreciable effect on stability behavior for the systems considered. The analyses conducted in this study indicate no clear benefit to using the DM when designing ductile steel systems in high seismic regions and simpler design methods may be equally effective.

To my Parents

ACKNOWLEDGEMENTS

First and foremost, I would like to express profound gratitude to my adviser Dr. Larry A. Fahnestock for giving me the opportunity to be a part of this project and providing me the necessary guidance and support along the way. I greatly appreciate the way he encouraged me to delve into complex issues and patiently allowed me to learn and work at my own pace. I am inspired by his attention to detail and his intense commitment to work. I have thoroughly enjoyed working with him and am thankful for his support both at an academic and personal level.

I am deeply indebted to my parents who motivated me to pursue graduate studies at Illinois, without their support I may not have come here. I also want to thank my two elder sisters for their constant encouragement throughout my academic life. I am grateful to Dr. Sudhir Misra and Dr. K.K. Bajpai, my mentors at IIT Kanpur (India), who were instrumental in getting me interested in structural engineering research. Special thanks go out to: Matthew Parkolap, Evgueni Filipov and Joshua Steelman for helping me tackle technical challenges during the course of this work. I will cherish the past two years at Illinois for the rest my life.

The work described in this dissertation was conducted as part of an ASCE/SEI special project entitled “Interface of the Direct Analysis Method and Seismic Design Requirements.” This project is being conducted under the Technical Committee on Methods of Design (TAC Metals) and I would like to thank the committee members for input throughout the course of this research. In particular, the advice of Prof. Donald W. White of Georgia Tech, past chair of the committee, is gratefully acknowledged. The computational simulations described herein were conducted in part using an allocation through the TeraGrid Advanced Support Program. All opinions, findings, and conclusions expressed are those of the author.

TABLE OF CONTENTS

CHAPTER 1
INTRODUCTION

1.1 Motivation

In the 2010 American Institute of Steel Construction (AISC) *Specification for Structural Steel Buildings* (AISC 2010a), hereafter called the *Specification*, the Direct Analysis Method (DM) is the standard stability analysis and design method. Compared to older methods, such as the Effective Length Method (ELM), the DM accounts for the critical factors that affect stability of steel buildings in a more transparent manner. Accounting for these factors, which include geometric nonlinearity, initial geometric imperfections, and inelastic behavior due to residual stresses, allows the effective length factor, K, to be set equal to 1 in column strength calculations. Research conducted over the course of nearly twenty years (e.g. Liew et al. 1994, White and Hajjar 1997 and 2000, Surovek-Maleck and White 2004a and 2004b, White et al. 2006) has shown that these two effects can have an appreciable impact on stability behavior in design scenarios that do not contain seismic loading.

While the DM could potentially be applied to seismic design, the interface between the DM, steel seismic provisions and seismic design requirements in *Minimum Design Loads for Buildings and Other Structures: ASCE/SEI 7-10* (ASCE 2010), hereafter called *ASCE-7*, is not fully established. The commentary to the 2010 AISC *Seismic Provisions for Structural Steel Buildings* (AISC 2010b), hereafter called the *Seismic Provisions*, states that the DM is not intended "to ensure stability under seismic loads where large inelastic deformations are expected." This is because seismic design was not considered in the development process of the DM. Thus, it is critical to explore the impact of the key issues that undergird the DM, namely,

geometric nonlinearity, initial geometric imperfections, and inelastic behavior due to residual stresses on the seismic behavior of typical steel buildings before the DM is extended to seismic design.

This research draws motivation from the issues presented above and aims to address the interface of current seismic design and non-seismic stability design requirements. The study provides a detailed assessment of the impact of residual stresses and initial imperfections on the nonlinear behavior of typical steel buildings that were designed for seismic loading. The study also explores the basis for extending the DM to design of ductile steel earthquake-resisting systems (like special moment-resisting frames) and makes recommendations for improving the state of the design practice for such systems.

1.2 Need for the Direct Analysis Method

Prior to 2010, the Effective Length Method (ELM) was the standard stability design procedure in the AISC *Specification*. In the ELM, effects of residual stresses and initial imperfections are accounted for in two ways. The column strength curve is calibrated to include the effects of residual stresses and initial geometric imperfections. Additionally, interactions between the global frame behavior and that of its members are handled approximately through the use of effective length factors (*K*-factors). Simply put, the *K*-factor is used to represent the influence of the system on the strength of an individual member. This approach allows the engineer to isolate a member from the system and design it based on strength curves and interaction equations developed for them. However, this approach does not satisfy compatibility between the actual inelastic member at the strength limit state and the elastic system as assumed in the frame analysis.

In many instances, the calculation of *K*-factors is not trivial. Although 'alignment charts' are provided by the AISC *Specification* (AISC 2010a) to assist the engineer in calculating *K*-factors, these charts have been developed for highly idealized scenarios which are rarely encountered in design practice. Moreover, these charts do not account for the leaning column effect and the commentary to the AISC *Specification* suggests a corresponding adjustment to *K*-factors which involves further approximations. Thus, for complex systems, engineers prefer to develop representative buckling models to obtain *K*-factors from corresponding elastic buckling loads. The development of appropriate buckling models requires significant engineering judgment and researchers (e.g. Maleck and White 2000) have demonstrated several complications associated with this process.

Through benchmark studies, Maleck (2001) showed that for non-redundant structures that have significant second-order moment amplification, the system strength can be substantially underestimated by using the ELM. The benchmark studies also demonstrated that by ignoring imperfection effects in second-order analysis, the ELM can substantially underestimate the maximum column end moment in some cases. Moreover, in lateral load resisting systems with low gravity to lateral load ratio, beam end moments can be significantly underestimated.

The factors discussed in this section highlight the need for an a stability design procedure that explicitly evaluates the behavior of the system and its members together and overcomes shortcomings of the ELM in a rational manner. This led to development of the DM.

1.3 Development of the Direct Analysis Method

Within the framework of second-order elastic analysis, the research done to develop the DM focused on simplified approaches to capture the effects of initial geometric imperfections

and inelastic behavior due to residual stresses. As a result, in the DM, initial geometric imperfections are represented by notional loads, although direct modeling of initial imperfections is also permitted, and inelastic behavior due to residual stresses is represented by stiffness reduction. This section explores the rationale behind the *three design-analysis constraints* of the DM prescribed by the AISC *Specification* (AISC 2010a).

1.3.1 Modeling of Geometric Imperfections

It is generally acknowledged that geometric imperfection effects, namely 1) member out-of-straightness and 2) frame out-of-plumbness, should be incorporated in a second-order analysis.

1.3.1.1 Member Out-of-Straightness

The modeling of member out-of-straightness within an analysis of the overall structural system, either directly or using notional loads (Liew et al. 1994), is highly cumbersome. White & Nukala (1997) suggested that a limit of

$$\frac{P_u}{P_e} < \frac{1}{7} \tag{1.1}$$

where $P_e = \dfrac{\pi^2 EI}{L^2}$

is sufficient to restrict the reduction in strength due to out-of-straightness to less than 5% for a wide range of section types. Further, in unbraced moment-resisting frames, the beam-columns are rarely loaded beyond this limit. Thus, based on these suggestions, the *first design-analysis constraint* of the DM permits the effects of member out-of-straightness to be neglected provided

the axial loads in all members contributing to the lateral stability of the structure satisfy the following limit:

$$P_u < 0.15P_e(\approx \frac{P_e}{7}) \tag{1.2}$$

In members that do require directly modeling of the out-of-straightness, it has been deemed appropriate to use a sinusoidal shape with a maximum value of L/1000 at the center as specified by the AISC *Code of Standard Practice for Steel Buildings and Bridges* (AISC 2010c), hereafter called the *Code of Standard Practice*.

1.3.1.2 Frame Out-of-Plumbness and Frame Nonverticality

Imperfections associated with frame out-of-plumbness are due to erection tolerances and include both story out-of-plumbness and overall frame nonverticality. The *Code of Standard Practice* (AISC 2010c) specifies a tolerance of 1/500 on the initial story out-of-plumbness ratio for low to medium rise buildings. Bridge (1998) suggested that only two imperfection patterns need to be considered, a uniform nonverticality of e_{oh}/H over the full height of the structure where e_{oh} is the allowable tolerance for frame nonverticality, or a local story imperfection of H/500 in a single "critical story." An equivalent horizontal or notional load of 0.002 ΣQ at each story level, where ΣQ is the total gravity load on a story, will produce accurate results when compared to those produced by directly modeling an H/500 imperfection. Kim (1996) recommends the use of a "further reduced tangent modulus" of 0.85E in lieu of direct modeling of imperfections or the use of notional loads.

To identify an appropriate modeling technique for capturing the frame out-of-plumbness effect, Maleck (2001) conducted a parametric study using the following three methods of

modeling imperfections: (1) explicit modeling of nominal geometric imperfections; (2) use of equivalent notional lateral loads; and (3) use of a reduced elastic modulus. It was concluded that explicit modeling, or equivalently, including notional loads captured frame behavior fairly well. However, implicitly modeling imperfections with a reduced modulus over-predicted strength when compared to direct modeling and this could be unconservative in gravity load cases. Based on these findings, the *second design-analysis* constraint of the DM permits either direct modeling of initial out-of-plumbness, assuming an initial out-of-plumbness ratio of 1/500, or application of notional loads equal to 0.002 Y_i at each story level, where Y_i is the total gravity load acting on that story. Further, it permits the use of a smaller nominal out-of-plumbness where justified based on project-specific requirements.

1.3.2 Modeling of Residual Stresses

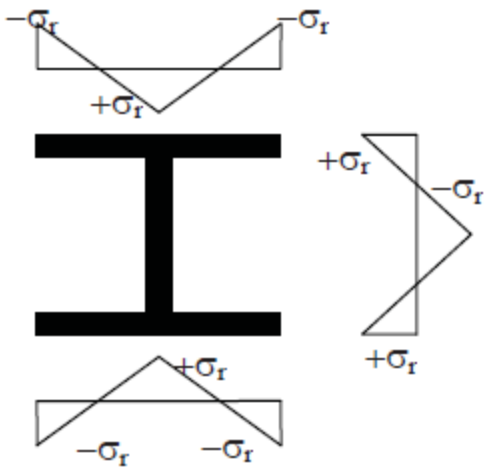

Figure 1.1 - Typical residual stress pattern for an I-shaped steel member

Thermal residual stresses are present in steel members due to uneven cooling after the rolling or welding process. In an I-shaped member, the residual stress distribution shown in Figure 1.1 is a consequence of extreme fibers of the section, with ample surface area, cooling

first. When the remaining portions of the section cool, their contraction is prohibited by those elements that have already cooled, and the net result is a section with built-in compressive and tensile stresses.

When external compressive loads are applied on such a section, yielding occurs first in the portions which are under compressive residual stresses. Thus the presence of residual stresses affects spread of plasticity in the section and there is a softening of the stress-strain response of the member. To account for this softening, the *tangent modulus buckling theory* assumes that the yielded portions do not contribute to the flexural stiffness and the observed behaviour can be approximated with an *effective flexural stiffness* EI_{eff}, computed from the elastic stiffness of the non-yielded portions only. Since this stiffness represents a *reduced elastic section*, it is lower than the flexural stiffness based on the gross section. This is how an *effective stiffness reduction* is attributed to the presence of residual stresses in steel sections.

1.3.2.1 Stiffness Reduction in the DM:

The *third design-analysis constraint* of the DM requires that the analysis be based on a reduced stiffness:

$$EI^{*} = 0.8\tau_b EI \tag{1.3}$$

where:

$\tau_b = 4\frac{P_u}{P_y}(1-\frac{P_u}{P_y})$ for $P_u > 0.5P_y$

$\tau_b = 1$ otherwise

Stiffness reduction is primarily based on the *column inelastic stiffness reduction factor* (**SRF** or $\boldsymbol{\tau}$) that corresponds to the *column strength curve* in the AISC *Specification* (AISC 2010a). The design check for compression members can be represented by:

$$P_u < \phi P_n = \phi \frac{\pi^2 EI_{eff}}{L^2} = \phi\tau \frac{\pi^2 EI}{L^2} \tag{1.4}$$

where

$$\tau = -2.724 \frac{P_u}{P_y} \ln(\frac{P_u}{P_y}) \quad \text{for} \quad P_u > 0.39 P_y$$

$$\tau = 1 \quad \text{otherwise}$$

Thus, SRF (τ) is ratio of rigidity of the effective column elastic core $(EI)_{\text{eff}}$ to elastic rigidity of the cross section (EI), and it accounts for stiffness reduction due to geometric imperfections and spread of plasticity due to residual stresses.

For slender members the *column curve equation*, E3-3 in the AISC *Specification* (AISC 2010a), further suggests a reduction factor of *0.877*, which along with $\phi = 0.9$, implies:

$$\phi P_n = 0.9(0.877)\tau \frac{\pi^2 EI}{L^2} = 0.79\tau \frac{\pi^2 EI}{L^2} \approx \frac{\pi^2 (0.8\tau EI)}{L^2} \tag{1.5}$$

Thus, for slender members, where the limit state is governed by elastic stability, the (0.8τ) reduction factor on stiffness results in a system available strength equal to (0.8τ) times the elastic stability limit. Although the 0.877 factor does not apply for frames with intermediate or stocky columns, it can be argued that by using the same (0.8τ) factor it is possible to account for inelastic softening that occurs prior to the members reaching their design strength. Therein lies

the idea that by modifying stiffness by a factor of (0.8τ) in the analysis, it is possible to check the beam-column interaction for in-plane flexural buckling by using an axial strength P_n calculated from the *column curve* and by using the actual unbraced member length L, i.e. with K-factor equal to 1.0.

In benchmark studies presented by Maleck (2001) and summarized by Surovek-Maleck and White (2004a and 2004b), stiffness reduction in the analysis was first implemented as a part of the proposed *Modified Elastic Approach*. It was observed that factoring the SRF (or ***τ)*** values by *0.9* for strong-axis bending and *0.8* for weak-axis bending produces accurate nominal beam–column strength predictions over a full range of moment to axial load ratios for a comprehensive set of frame and member benchmark problems. Thus, equivalent uniform flexural rigidities, $EI_{eff} = 0.9\tau EI$ for strong-axis bending and $EI_{eff} = 0.8\tau EI$ for weak-axis bending were suggested.

However, while developing the DM for implementation in the AISC *Specification*, a single value was chosen for both strong and weak axis bending, again for the sake of simplicity. Further, a modified expression for τ was chosen based on the conventional Column Research Council (CRC) *column strength formula* (SSRC 1976). A reason for this choice could be that the CRC formula is a tangent modulus expression that does not include the effects of geometric imperfections (Lu et al. 2009). Thus, a τ-value based on CRC (i.e. τ_b in DM) represents effects of distributed plasticity due to residual stresses only while the SRF includes effects of both residual stresses and member-out-of-straightness. Consequently, τ_b is slightly greater than SRF (τ), as shown in Figure 1.2.

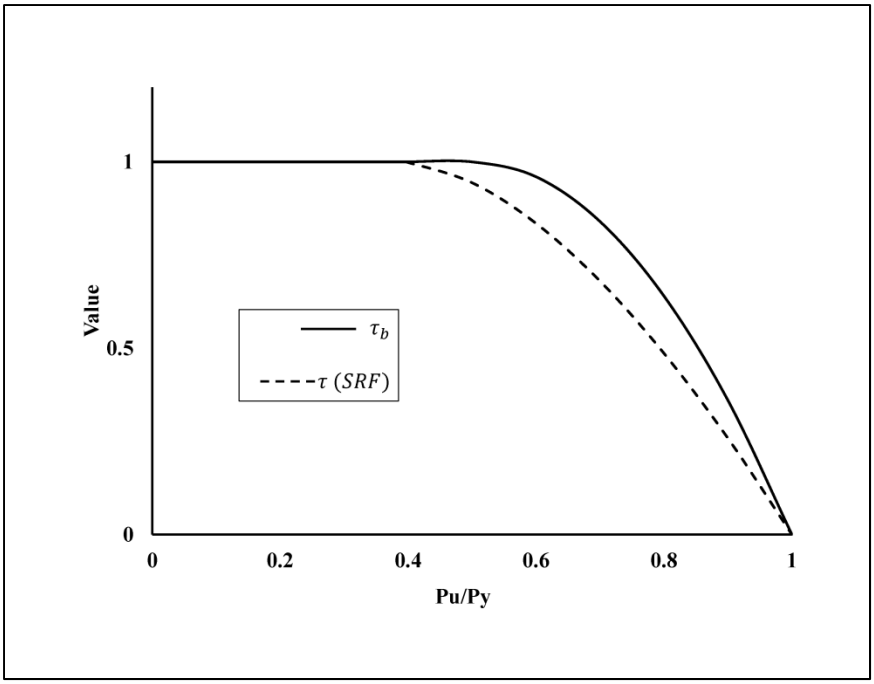

Figure 1.2 - Comparison of τ_b (DM) and column inelastic stiffness reduction factor (SRF)

1.4 Benefits of the Direct Analysis Method

The previous section presented the rationale behind the provisions of the DM. It is evident that the DM accounts for factors affecting inelastic frame behavior in a more transparent manner compared to the ELM. Verification studies presented by Maleck (2001), Surovek-Maleck and White (2004b) and White et al. (2006), show that the DM has been calibrated to directly evaluate frame behavior at the ultimate strength level, as determined using distributed plasticity analysis. In other words, frame response obtained using the DM is represented by an approximate secant stiffness to the ultimate strength level.

Thus, it can be said that the adjustments to the elastic analysis model prescribed by the DM, combined with an accurate calculation of the second-order effects, lead to an improved representation of the second-order inelastic forces in the structure at the ultimate strength limit. Due to this improved representation of internal forces, column nominal strength for checking in-

plane resistance can be based on the actual unsupported length in the plane of bending thereby eliminating the need for *K*-factors. Applying $K = 1$ for in-plane stability design is a significant advantage that the DM offers to the design practice for reasons discussed in section 1.2.

In addition to elimination of *K*-factors from the design process, Maleck (2001) demonstrated that unlike the ELM, using the DM does not lead to underestimation of end moments in columns and beams in structural systems which are sensitive to imperfection effects as well as effects of distributed plasticity within the system. Surovek-Maleck and White (2004b) have also shown that the DM can lead to more economical beam-column proportions in certain cases. Lastly, the DM applies in a logical and consistent fashion for all frame types – moment-resisting frames, braced frames, combined systems and thus for all these reasons it has become the preferred stability design procedure in the latest AISC *Specification* (AISC 2010a).

1.5 Scope and Organization

1.5.1 Research Needs

The research which led to the development of the DM has shown that it can play a major role in stability-sensitive frames where gravity loads are the dominant loadings. But, many questions arise concerning application and adaptation of the DM to seismic design. For instance, the commentary of the AISC *Specification* (AISC 2010a) states that the DM should not be used for stability analysis in scenarios involving large inelastic drifts. However, ductile earthquake-resisting systems may be governed by drift-limits and thus have significant system overstrength. Also since the DM was calibrated at ultimate strength levels under non-seismic loadings, it is unclear whether the DM could suitably represent structural behavior at other load levels. Moreover, factors like member overstrength, which are inherent to seismic design, were not

considered in the research that led to the development of the DM. These issues need to be addressed before the DM can be rationally extended to seismic design.

1.5.2 Research Objectives

The objective of this research is to evaluate the relevance of the DM in the context of seismic design of steel special moment-resisting frames (SMRFs). For this purpose, it is critical to explore the impact of the two basic features of the DM, namely initial geometric imperfections and residual stresses, on nonlinear behavior of SMRFs. Amongst the various lateral load-resisting systems, SMRFs are highly dependent on ductile inelastic behavior for earthquake resistance and are hence drift-sensitive. It is therefore expected that evaluating the DM with respect to SMRFs will give a fair idea about the role which the DM could play in the realm of seismic design of ductile earthquake-resisting systems.

1.5.3 Research Scope

To achieve the research objectives a series of steel SMRF models were subjected to monotonic pushover, cyclic pushover and response history analyses in the present study. These frames were extracted from 3, 9, and 20-story buildings designed for three U.S. locations representing different levels of seismicity: Los Angeles, Seattle, and Boston. The observed behavior was used to draw comparisons between systems with and without residual stresses and initial imperfections. Cyclic strength degradation behavior was also incorporated to study the relative importance of this effect in comparison to the effects of residual stresses and initial imperfections.

1.5.4 Thesis Outline

This dissertation has been organized as outlined below:

- Chapter 2 describes the development of numerical models for the steel frames and provides details about the three main analyses used in this study.
- Chapter 3 presents results of the three analyses and highlights the observed effects of residual stresses and initial imperfections
- Chapter 4 discusses the observed behavior when cyclic strength degradation at beam-column connections was incorporated to examine the potential interaction it may have with other parameters in the DM.
- Chapter 5 presents a summary and conclusions of the research and suggests potential implications of this work on the design practice.

CHAPTER 2
MODELING AND ANALYSIS PROCEDURES

2.1 Building Numerical Models

Steel moment-resisting frames that were designed for the SAC project (FEMA 2000) were analyzed in the present research. The frames were extracted from 3, 9, and 20-story buildings designed for three U.S. locations representing different levels of seismicity: Los Angeles, Seattle, and Boston. The frames are named by location and height: Boston (BOS-3, BOS-9 and BOS-20), Seattle (SEA-3, SEA-9 and SEA-20) and Los Angeles (LA-3, LA-9 and LA-20). All buildings have special moment-resisting frames (SMRFs) along the perimeter column lines and amongst these the N-S frames were used in the present study. The frame layout, dimensions, section sizes, weight, and additional details of the structures considered in the present research were based on the pre-Northridge design models reported by Gupta and Krawinkler (1999). These prototypes were chosen since they represent relatively modern designs, yet they lack the post-Northridge modifications and as such, they may be slightly more prone to seismic instability. Appendix A provides the dimensions and section sizes for all the nine frames used in this study (T. Okazaki, unpublished internal report, November 2008).

Numerical models for the prototype buildings were developed in OpenSees (Mazzoni et al. 2009), which is a software package that incorporates geometric and material nonlinearity. Accuracy of the second-order analysis was confirmed using the benchmark problems presented in the Commentary to the *Specification* (AISC 2010a). A basic centerline approach was adopted to build all the numerical models, with beams and columns meeting at a beam-to-column node. All the elements within these models were nonlinear beam-column elements with fiber cross

sections using a yield stress of 55 ksi and strain hardening coefficient of 2%. For the sake of simplicity and consistency with research that developed the DM, panel zones, composite slabs, and doubler plates were not incorporated in the models.

Due to absence of any irregularities in the buildings, 2-D analysis was sufficient for the purpose of this study. Moreover, because of symmetry in the building, it was assumed that tributary mass for one of the N-S frames would be half of the total building mass. The gravity system was represented by a leaning column, whose floor level nodes were constrained to move in the lateral direction with other frame nodes at that floor level. The leaning column was pinned at the top and bottom of each story and therefore did not contribute to lateral load resistance. The loads and masses were determined and applied based on the details provided by Gupta and Krawinkler (1999). In order to obtain a sufficient level of accuracy from the analysis, each individual member in a frame was divided into 8 elements (Lamarche and Tremblay, 2008).

In selected cases, geometric imperfections and residual stresses were incorporated in the frame models. Geometric imperfections were modeled explicitly by providing an initial story drift (story displacement divided by story height) of 1/500 directly in the numerical model. For the taller frames, the initial story drift was introduced in the bottom stories up to the floor where the maximum envelope permitted by the AISC *Code of Standard Practice for Steel Buildings and Bridges* (AISC 2010c) was reached. The initial story drift was always placed in the positive direction as defined in the results presented in Chapter 3. A co-rotational coordinate transformation was used for all column elements to ensure geometric non-linear effects were included. Beam elements used a P-Delta transformation due to the incompatibility of distributed loads with the co-rotational formulation in OpenSees.

To add the effects of residual stresses, features of the Steel02 material model in OpenSees were utilized. The Steel02 material represents the uniaxial Giuffré-Menegotto-Pinto constitutive model for steel with isotropic strain hardening (Menegotto and Pinto 1976, Filippou et al. 1983). It allows for the assignment of an initial stress to the material. Thus, a residual stress distribution was created based on the pattern proposed by Galambos and Ketter (1959) and each fiber was assigned an initial stress. Figure 2.1 depicts the fiber discretization and the residual stress patterns used in this study.

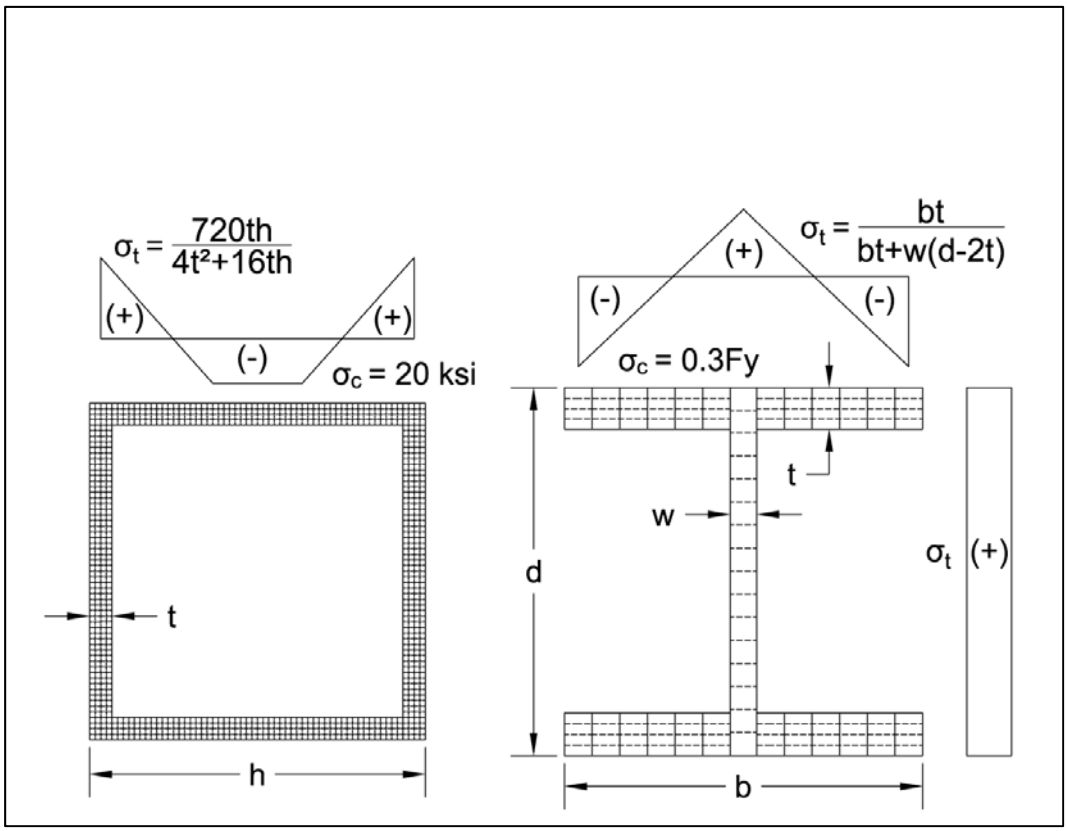

Figure 2.1 – Fiber discretization and residual stress patterns (dashed and solid lines represent fiber and patch boundaries respectively)

As shown in Figure 2.1, flanges of I-shaped members were discretized into 12 quadrilateral patches along their length, with different initial stresses symmetrically assigned to the patches. The 12 patches were subdivided further into 4 fibers each. Over the depth of the

web, 16 fibers were used and all the fibers were assigned the same initial stress. Square HSS sections in LA-20 were discretized into 15 quadrilateral patches along the length of each side, with each patch subdivided further into 16 fibers. Similar to flanges in I-shaped members, fibers within the same patch were assigned the same initial stress however the stress distribution varied along the length of a side. A peak compressive stress of 20 ksi was assumed to be distributed over the middle third of the section's width, with a linear distribution (for simplicity) up to the peak tensile stress, determined as a function of the thickness and width of the section such that the total resultant force was zero (Salmon et al. 2009).

2.2 Analyses

Three different types of analysis were conducted for each frame to observe the effects of residual stresses and geometric imperfections on system behavior.

2.2.1 Nonlinear Static Analysis

The nonlinear static procedure, colloquially referred to as "pushover analysis", has become a popular tool in engineering practice for evaluating the safety of structures against an earthquake-induced collapse. The purpose of such an analysis is to obtain a base shear versus lateral drift relationship by subjecting a structural model to a prescribed heightwise distribution of lateral forces. Pushover analysis provides information regarding inelastic behavior characteristics of the structure without going to a more complex response history (or "dynamic") analysis. Studies have shown that pushover analysis can provide a reasonable estimate of the deformation demands in structures that respond primarily in the first mode (Gupta and Krawinkler, 1999). In the present research two types of pushover analysis were conducted: monotonic and cyclic.

2.2.1.1 Monotonic Pushover Analysis

Monotonic pushover analysis was performed on each frame to evaluate lateral strength and stability. First, constant gravity loads, $D + 0.25L$, were applied. Second, the frame was pushed laterally under displacement control using simulated horizontal earthquake loads until instability occurred or a global roof drift (lateral roof displacement divided by overall building height) of 0.1 rad was achieved. The loads were distributed over the height of the frame based on the equivalent lateral force procedure in *ASCE-7* (ASCE 2010). Thus, proportional loads were applied based on the vertical distribution factor, defined as follows:

$$C_{vx} = \frac{w_x \left(h_x\right)^k}{\sum_{i=1}^{n} w_i \left(h_i\right)^k} \tag{2.1}$$

where C_{vx} is the normalized load at floor level x, w_i and w_x are the seismic weights at floor i and x respectively, h_i and h_x are the heights from the ground level to floor i and x, and k is a period-dependent factor. In this study, a k value of *2* has been used for all pushover analyses as suggested by Gupta and Krawinkler (1999).

2.2.1.2 Cyclic Pushover Analysis

Although research supporting the development of the DM only considered monotonic response, seismic behavior is fundamentally related to cyclic response so it is an essential extension to examine the impact of initial imperfections and residual stresses on cyclic behavior. Thus, cyclic pushover analysis was also conducted for all nine prototype frames described above. Like in the monotonic pushover analysis, a constant gravity load defined by $D + 0.25L$ was first applied. Subsequently, proportional horizontal earthquake loads were applied using displacement

control such that the roof drift followed the history specified in the *Seismic Provisions* (AISC 2010b) for qualification testing of beam-to-column moment connections. The distribution of horizontal earthquake loads was again based on the equivalent lateral force procedure in *ASCE-7* (ASCE 2010) as described above.

2.2.2 Response History Analysis

Nonlinear response history analysis was also conducted using the prototype frame models to evaluate the dynamic behavior of these frames. Rayleigh damping was used based on 2% damping in the first and third modes. Representative sets of ground acceleration records for the three locations, which were assembled as part of the SAC steel project (Somerville et al. 1997), were used. These sets consisted of natural and synthetic records based on stiff soil conditions for return periods of 475 years (10% probability of being exceeded in 50 years, referred to hereafter as 10/50), and 2475 years (2% probability of being exceeded in 50 years, referred to hereafter as 2/50). Each set consisted of 20 acceleration records; 10 ground motions each with 2 orthogonal components. The sign of each record was chosen to maximize the drift response of the frame model with residual stresses and initial imperfections. Appendix B presents acceleration response spectra for the records that were used in the study.

CHAPTER 3
SIMULATION RESULTS

3.1 Introduction

Second-order distributed plasticity analysis was conducted under two different conditions. The baseline analysis case (called "base") did not include residual stresses and initial imperfections, while the modified analysis case (called "R-I") included residual stresses and initial imperfections. For each building location (LA, SEA and BOS) and height (3, 9 and 20), monotonic pushover analysis, cyclic pushover analysis and response history analysis were conducted under both R-I and base conditions. Results obtained from these analyses are discussed in this chapter.

3.2 Results for Monotonic Pushover Analyses

Monotonic pushover analyses for the frame models described in Chapter 2 were originally conducted by Okazaki et al. (2010). They have been briefly discussed here for the sake of completeness. Figure 3.1 and Figure 3.2 depict response for the LA-9 and BOS-9, respectively. In Figure 3.1(a), which plots normalized base shear vs. roof drift, it can be seen that for LA-9, the R-I and base cases matched very closely and only a slight difference can be observed in the post-peak range of behavior at large drift. The displacement profiles, which are shown in Figure 3.1(b), indicate that the plastic collapse mechanism was not concentrated in one story but rather distributed over multiple stories. The difference between the R-I and base cases is somewhat more pronounced for BOS-9, as shown in Figure 3.2. Behavior is similar prior to first yielding, but then the R-I case becomes softer and the ultimate base shear strength is

reduced by 2.5%. In the post-peak range of behavior, more deviation is observed in the displacement profiles as instability is triggered due to soft-story formation.

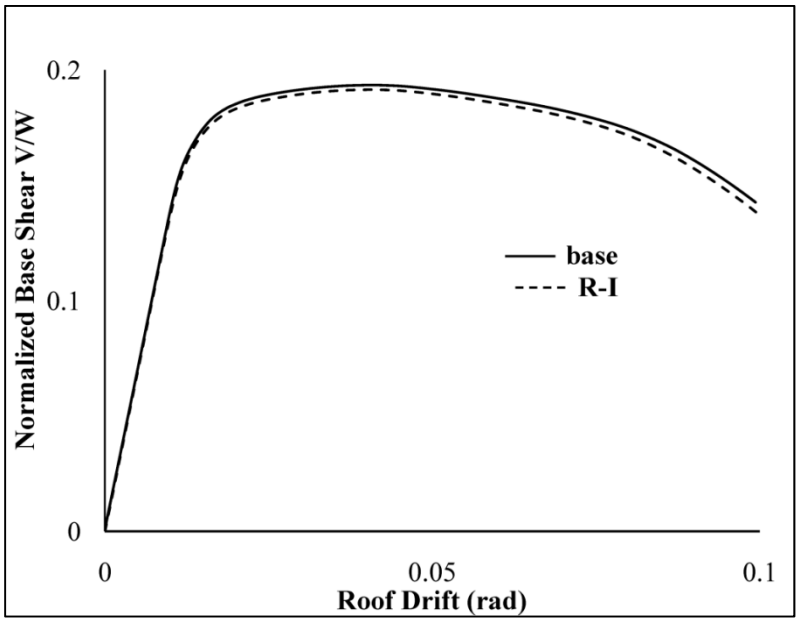

(a)

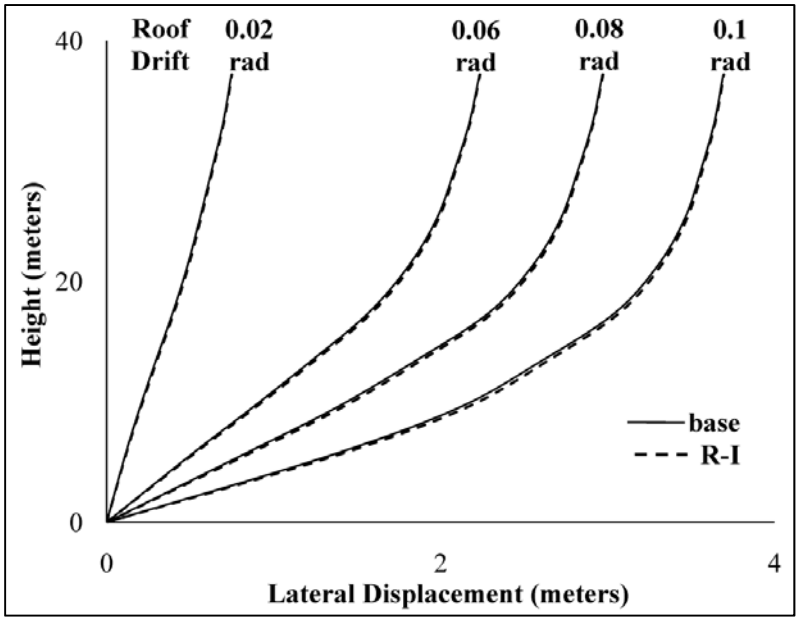

(b)

Figure 3.1 - Monotonic pushover response of LA-9: (a) normalized base shear vs. roof drift; (b) displacement profiles

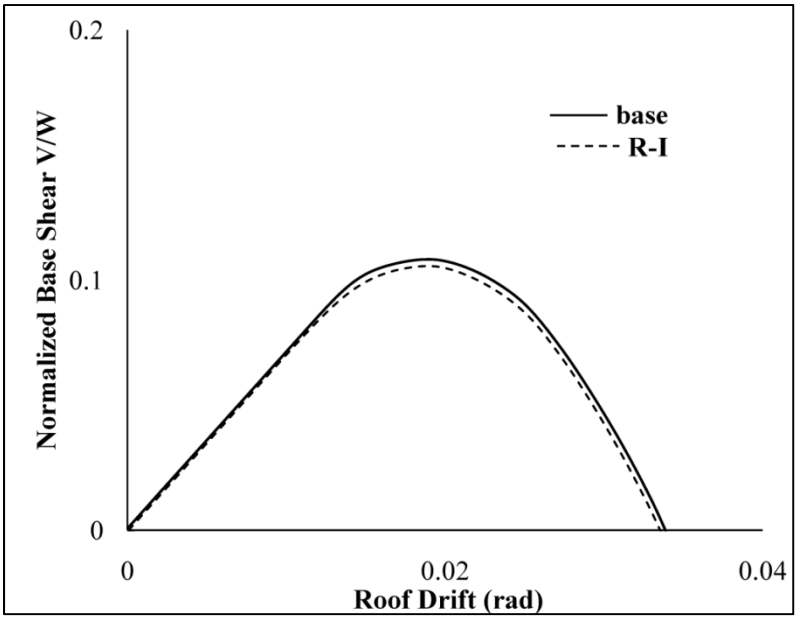

(a)

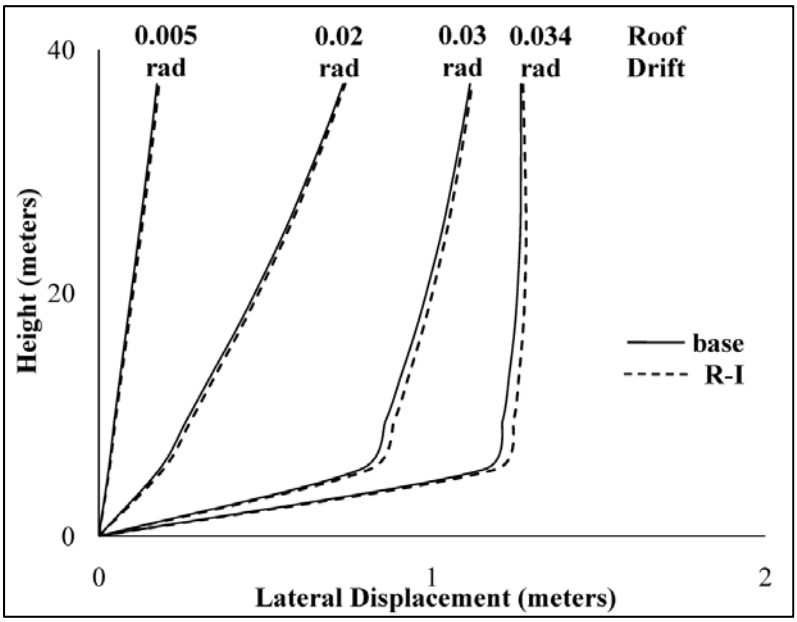

(b)

Figure 3.2 - Monotonic pushover response of BOS-9: (a) normalized base shear vs. roof drift; (b) displacement profiles

Thus, it can be seen that residual stresses and initial imperfections can play a role in structural stability behavior at large drift levels near collapse when soft-story response is

controlling the behavior. BOS-20 showed a behavior similar to BOS-9 while all the other 3, 9 and 20-story frames behaved in a manner which closely resembled to the response of LA-9.

3.3 Results for Cyclic Pushover Analyses

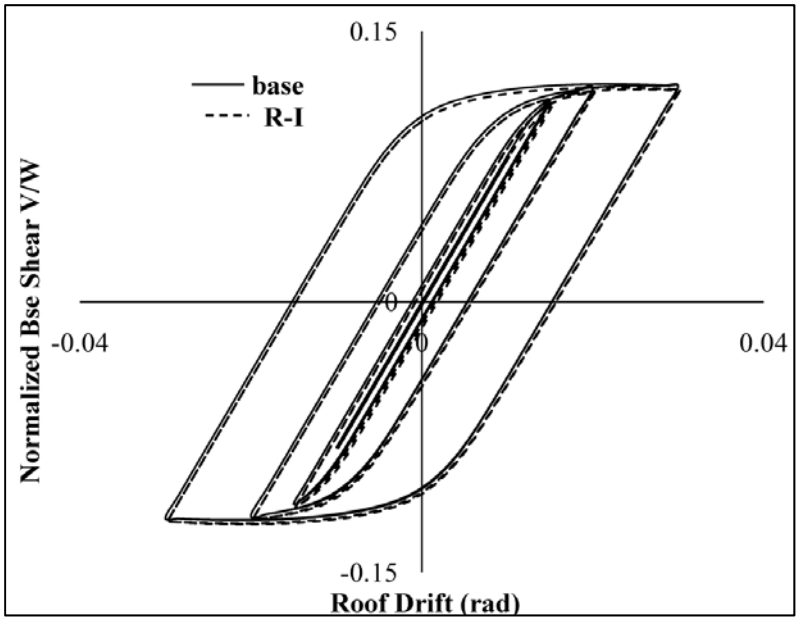

Figure 3.3 - Cyclic pushover response of BOS-3: normalized base shear vs. roof drift

Cyclic pushover analyses were again originally reported by Okazaki et al. (2010) and have been presented here for completeness. Figures 3.3 to 3.5 depict selected results from the cyclic pushover analyses to illustrate the range of behavior that was observed. Figure 3.3 compares the global cyclic response obtained for BOS-3 by plotting the relationship between normalized base shear and roof drift. It can be seen that cyclic response for the base and R-I models of BOS-3 matched very closely up to cycles of ±0.03 roof drift. The other 3-story frames (SEA-3 and LA-3) exhibited behavior very similar to BOS-3.

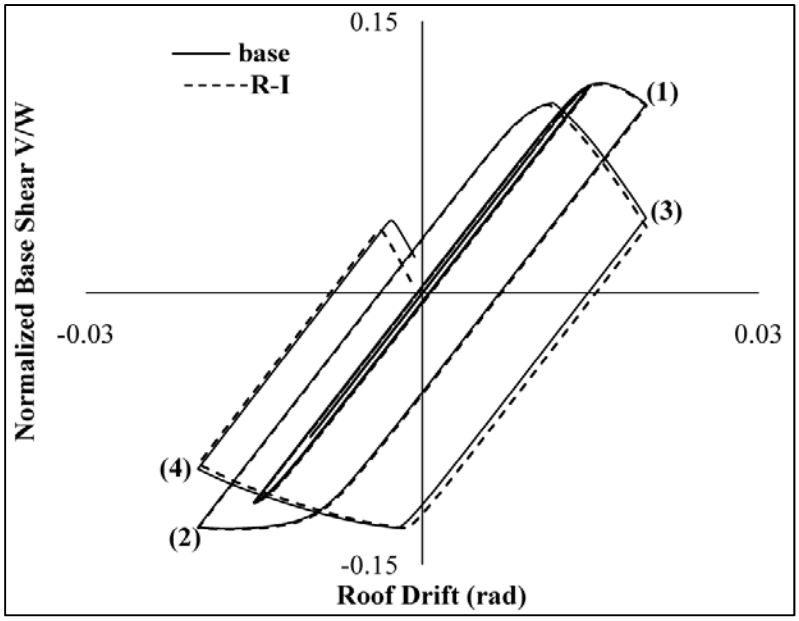

(a)

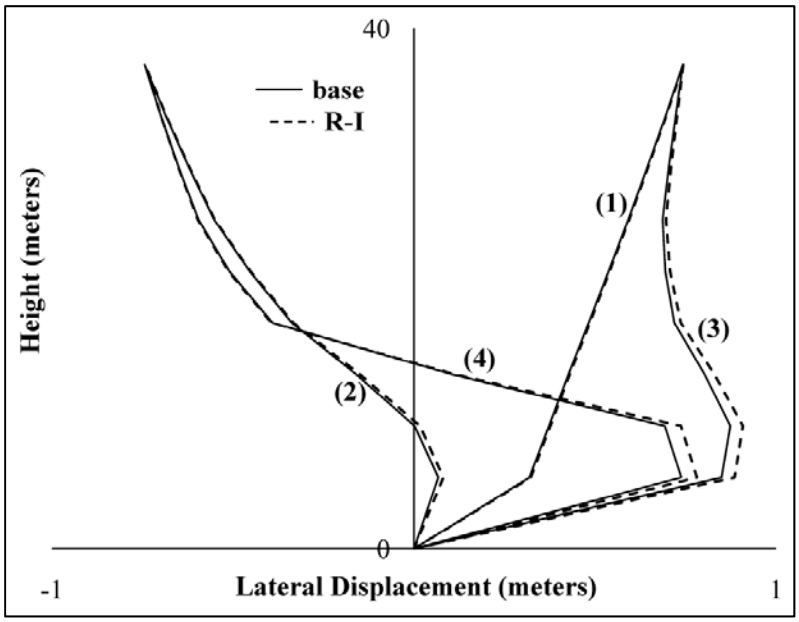

(b)

Figure 3.4 - Cyclic pushover response of BOS-9: (a) normalized base shear vs. roof drift; (b) displacement profiles

Close agreement between the R-I and base cases was also obtained for BOS-9, as seen in Figure 3.4(a), until soft-story behavior developed during the cycles of ±0.02 roof drift. Figure

3.4(b), shows displacement profiles for BOS-9 at four different stages in the cyclic response. As indicated in Figure 3.4(a), stages 1 and 3 were at the end of the first and second positive peaks at 0.02 roof drift, respectively, and stages 2 and 4 at the end of the first and second negative peaks at 0.02 roof drift, respectively. Figure 3.4(b) indicates that instability of BOS-9 was triggered by formation of a soft first story. At stage 1, the displacement profiles of the R-I and base models were nearly identical, but at stage 2, the lower half of the R-I model was not displaced as far in the negative direction by a small margin. Thus, when the loading was reversed to the positive direction in stage 3, a soft story formed earlier in the R-I model. By the time stage 4 arrived, collapse was impending. It is important to note that the two responses were nearly identical until softening behavior initiated during stage 2. The behaviors of SEA-9 and LA-9 were similar to BOS-3 in the sense that the R-I and base analyses were nearly identical and instability due to soft-story formation was not observed.

LA-20 experienced severe strength degradation and collapse during the roof drift cycles of ±0.03, as seen in Figure 3.5(a). The figure shows the normalized base shear versus roof drift response and displacement profiles at key stages. Figure 3.5(a) shows that at the first positive peak to 0.03 roof drift, notable strength degradation occurred. At 0.03 roof drift, the strength was 20% of the peak strength and very similar between the R-I and base cases. At the first negative peak to 0.03 roof drift, which is labeled stage 1 in Figure 3.5, a small deviation was observed between the R-I and base cases with the R-I case exhibiting slightly less negative displacement in the lower half of the structure and slightly higher strength, although strength degradation was again observed for both cases. At the second positive excursion to 0.03 roof drift, which is labeled stage 2 in Figure 3.5, story drift was fairly uniform for the bottom five stories, but the remaining fifteen stories had small story drifts.

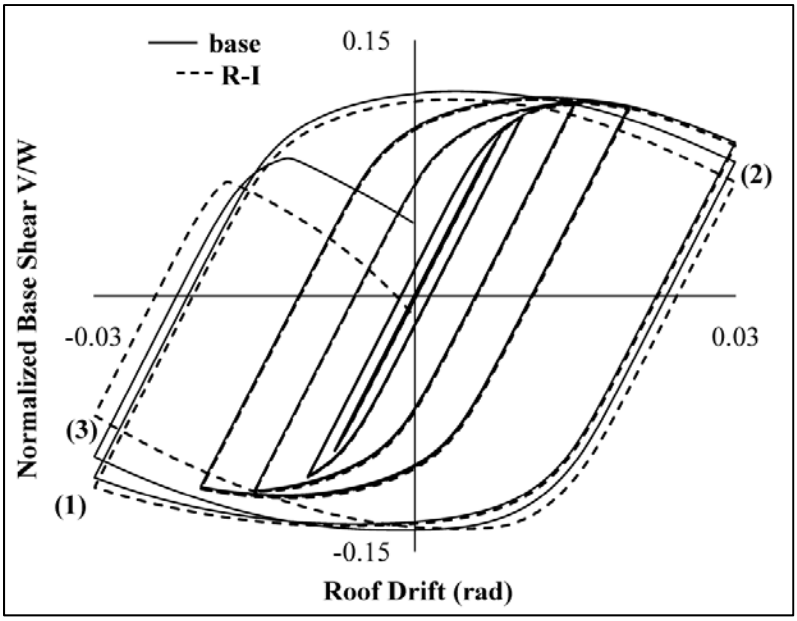

(a)

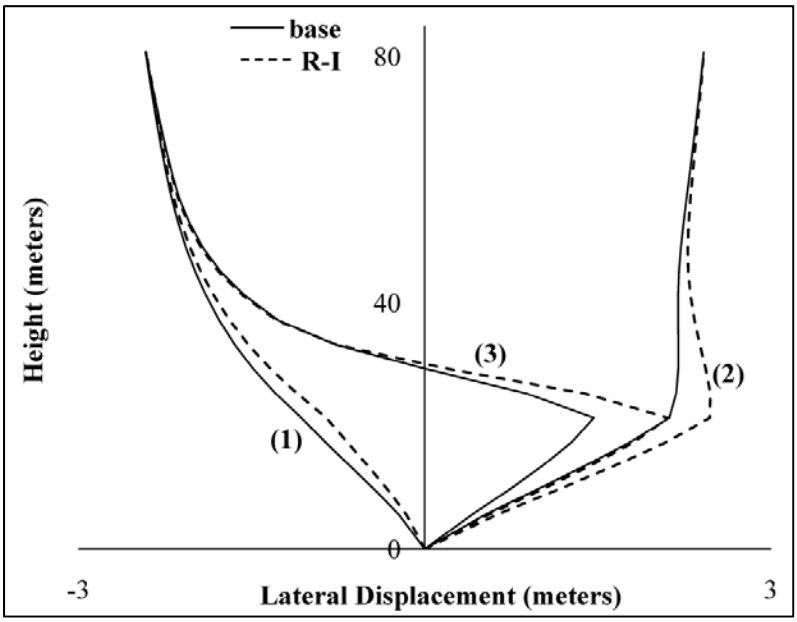

(b)

Figure 3.5 - Cyclic pushover response of LA-20: (a) normalized base shear vs. roof drift; (b) displacement profiles

This concentration of deformation, as seen in Figure 3.5(b), was observed for both R-I and base models of LA-20, although it is more pronounced for the R-I case. After loading was

reversed for the second excursion towards negative 0.03 roof drift, the difference between the R-I and base cases became more pronounced as the strength degradation was more severe for the R-I case. When the load was reversed towards positive drift, instability occurred due to the extreme story drifts in the lower ten stories. As Figure 3.5(a) illustrates, this instability occurred for both R-I and base cases, but it initiated at a slightly earlier stage in the R-I case. While SEA-20 showed a behavior very similar to the one described above, BOS-20 did not exhibit any strength degradation or instability.

These cyclic analyses show that models with residual stresses and initial imperfections experienced instability earlier than those without these effects. Further, it appears that the effects of residual stresses and initial imperfections on cyclic stability behavior are appreciable only after the peak lateral strength has been reached and global second-order effects become significant as story drift is concentrated in a few critical stories.

3.4 Results for Response History Analyses

Tables 3.1 and 3.2 summarize mean and mean plus one standard deviation response values for the base and R-I cases, when subjected to 10/50 and 2/50 ground motion sets respectively.

Frame	Value	base			R-I		
		Roof	Story	Residual Story	Roof	Story	Residual Story
LA-3	Mean	0.043	0.050	0.018	0.044	0.051	0.019
	Mean + St. dev.	0.065	0.074	0.038	0.066	0.074	0.039
SEA-3	Mean	0.042	0.052	0.019	0.043	0.053	0.022
	Mean + St. dev.	0.062	0.076	0.040	0.065	0.077	0.045
BOS-3	Mean	0.011	0.017	0.001	0.011	0.017	0.002
	Mean + St. dev.	0.014	0.023	0.003	0.014	0.023	0.004
LA-9	Mean	0.026	0.045	0.017	0.026	0.045	0.019
	Mean + St. dev.	0.037	0.072	0.037	0.037	0.074	0.039
SEA-9	Mean	0.018	0.023	0.007	0.018	0.024	0.008
	Mean + St. dev.	0.027	0.035	0.016	0.027	0.035	0.017
BOS-9	Mean	0.004	0.008	0.000	0.004	0.008	0.000
	Mean + St. dev.	0.007	0.011	0.000	0.007	0.011	0.000
LA 20	Mean	0.017	0.044	0.022	0.017	0.046	0.024
	Mean + St. dev.	0.027	0.079	0.054	0.027	0.083	0.059
SEA-20	Mean	0.009	0.016	0.004	0.009	0.016	0.005
	Mean + St. dev.	0.013	0.021	0.010	0.013	0.022	0.011
BOS-20	Mean	0.002	0.003	0.000	0.002	0.003	0.000
	Mean + St. dev.	0.004	0.005	0.000	0.004	0.005	0.000

Table 3.1 - Maximum drift quantities for response history analyses using 2/50 records

Frame	Value	base			R-I		
		Roof	Story	Residual Story	Roof	Story	Residual Story
LA-3	Mean	0.021	0.024	0.004	0.021	0.024	0.005
	Mean + St. dev.	0.028	0.031	0.008	0.028	0.031	0.009
SEA-3	Mean	0.016	0.022	0.002	0.017	0.022	0.002
	Mean + St. dev.	0.021	0.027	0.003	0.022	0.028	0.004
BOS-3	Mean	0.004	0.006	0.000	0.004	0.006	0.000
	Mean + St. dev.	0.005	0.008	0.000	0.005	0.008	0.001
LA-9	Mean	0.014	0.019	0.002	0.014	0.019	0.002
	Mean + St. dev.	0.018	0.026	0.004	0.018	0.026	0.004
SEA-9	Mean	0.010	0.013	0.001	0.010	0.013	0.001
	Mean + St. dev.	0.013	0.018	0.004	0.013	0.018	0.004
BOS-9	Mean	0.001	0.003	0.000	0.001	0.003	0.000
	Mean + St. dev.	0.002	0.004	0.000	0.002	0.004	0.000
LA 20	Mean	0.009	0.017	0.002	0.009	0.017	0.000
	Mean + St. dev.	0.012	0.025	0.004	0.012	0.026	0.005
SEA-20	Mean	0.005	0.009	0.001	0.005	0.009	0.001
	Mean + St. dev.	0.008	0.012	0.002	0.008	0.012	0.003
BOS-20	Mean	0.001	0.001	0.000	0.001	0.001	0.000
	Mean + St. dev.	0.001	0.002	0.000	0.001	0.002	0.000

Table 3.2 - Maximum drift quantities for response history analyses using 10/50 records

3.4.1 Response of 3-Story Frames

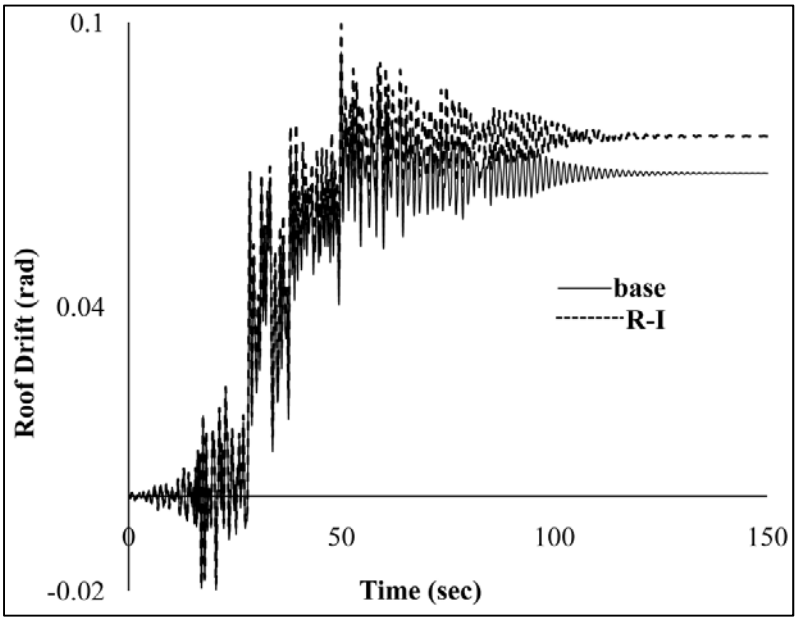

(a)

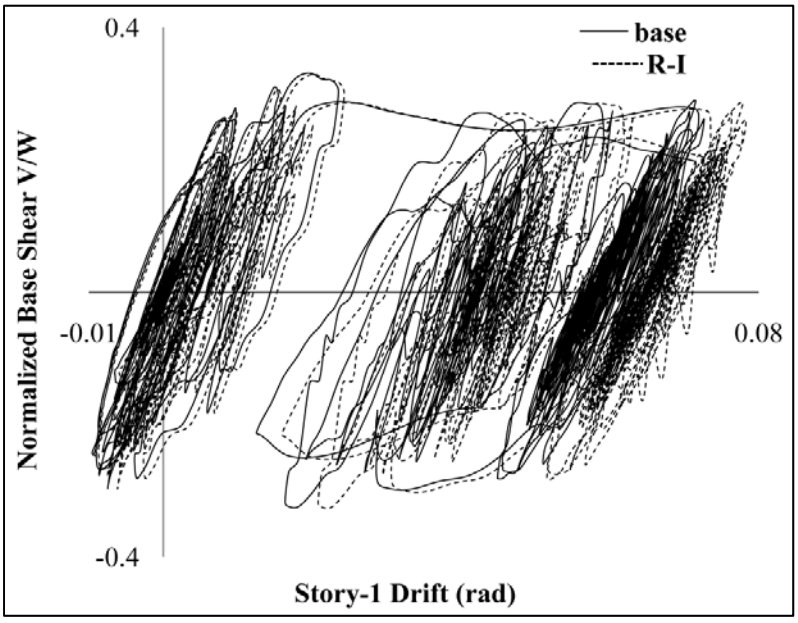

(b)

Figure 3.6 - Response history of SEA-3 for 'svlivna.n45' record: (a) roof drift vs. time; (b) normalized base shear vs. story-1 drift

Figures 3.6 depicts one of the most severe responses of a 3-story frame to a 2/50 record and it illustrates the differences that can occur between base and R-I cases. In Figures 3.6(a) and

3.6(b), roof drift versus time and first story shear versus drift are shown for SEA-3, respectively, under the 'n45' component of a 2/50 ground motion called 'svlvina' (svlivina.n45). It can be seen in Figure 3.6 that initially, for small drifts, the responses for the base and R-I cases were almost identical. However, for the strongest portion of the ground motion, the R-I case sustained larger inelastic response compared to the base case. As a result, the maximum story drift was 5% greater and the maximum residual story drift was 11% greater for the R-I case compared to the base case. However, as shown in Table 3.1, the story drift differential for SEA-3 was less than 3%, which is considerably smaller than the most severe case. Similar observations were made for LA-3, where only a small difference between base and R-I cases was observed.

Tables 3.1 and 3.2 show that drifts obtained for BOS-3 were much lower than LA-3 and SEA-3. Moreover, the standard deviation in drifts for BOS-3 was also very small implying that predominantly low drifts were obtained for both 2/50 and 10/50 records. Figure 3.7 depicts a typical response history for BOS-3. In Figures 3.7(a) and 3.7(b), roof drift versus time and first story shear versus drift are shown for BOS-3, respectively, under the 'n45' component of a 2/50 ground motion called 'bsgsm08' (bsgsm08.n45). It can be seen in Figure 3.7(a) that the maximum roof drift was slightly greater than 0.01 rad and the difference between maximum roof drifts for the base and R-I cases was nearly 2%. Figure 3.7(b) reveals that since the response of BOS-3 was predominantly elastic and the ground motion did not cause any severe inelastic drifts in the frame. Thus, in the absence of any large inelastic excursions both the base and R-I cases closely matched each other.

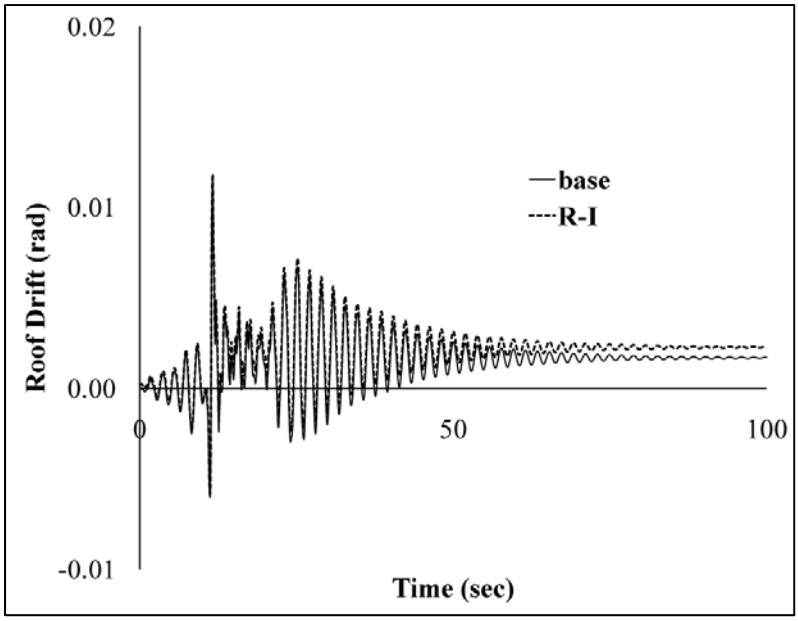

(a)

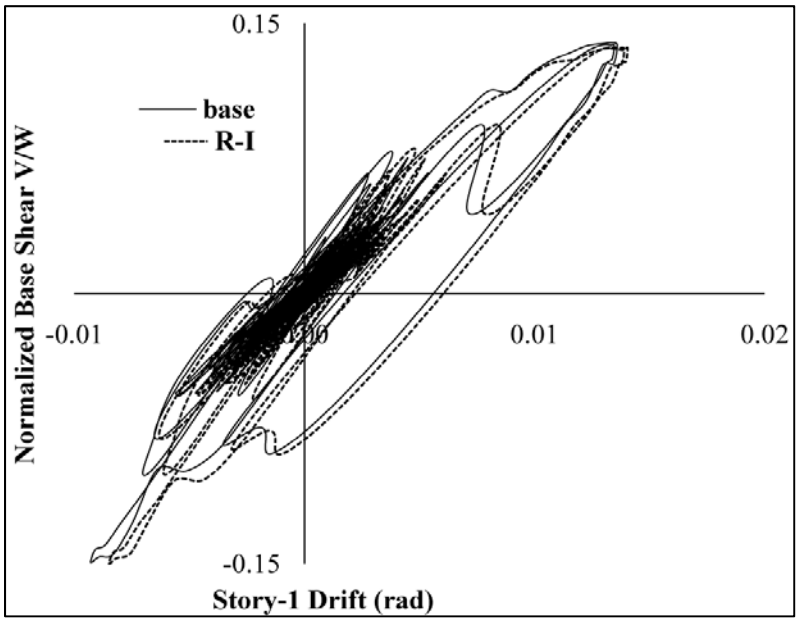

(b)

Figure 3.7 - Response history of BOS-3 for 'bsgsm08.n45' record: (a) roof drift vs. time; (b) normalized base shear vs. story-1 drift

3.4.2 Response of 9-Story Frames

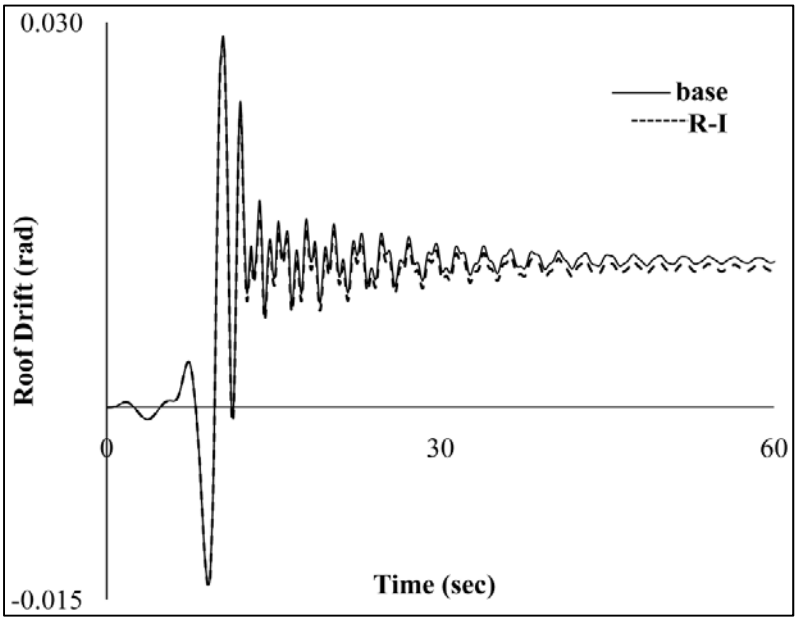

(a)

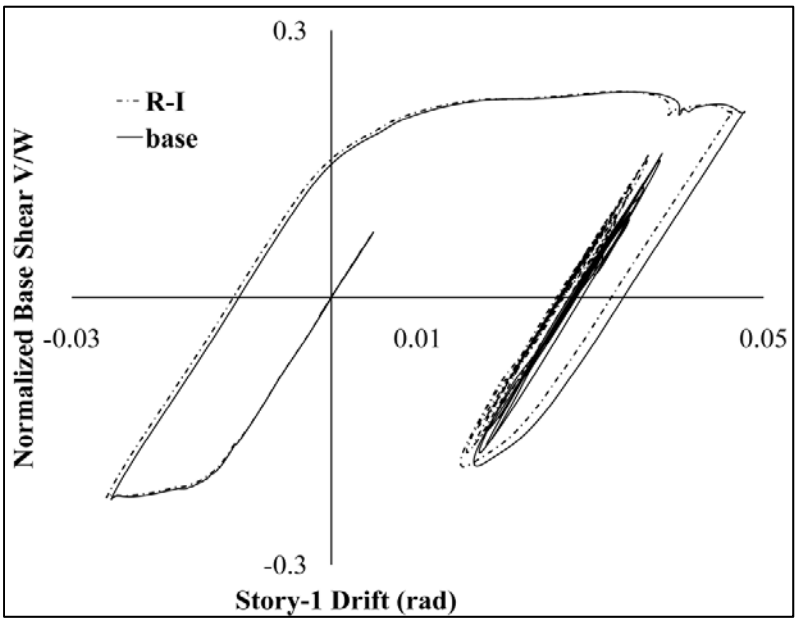

(b)

Figure 3.8 - Response history of LA-9 for 'lepst10.p45' record: (a) roof drift vs. time; (b) normalized base shear vs. story-1 drift

Figure 3.8 illustrates results for LA-9 obtained using a 2/50 ground motion 'lepst10.p45'. Although the difference between the base and R-I cases was not prominent, this case is of

interest since the drift response was smaller for the R-I case. It is intuitive to expect that the effective softening due to residual stresses and geometric imperfections will cause drifts in the R-I case to be larger than in the base case. However, during the first inelastic excursion in the negative direction, the R-I case was pushed further in the negative direction and thus when a large inelastic excursion occurred in the positive direction, the R-I case was initially biased in the negative direction and experienced a smaller maximum positive response than the base case. Thus, due to larger inelastic deformation in one direction, the R-I case experienced smaller drifts in the other direction when the loading reversed. In effect, the R-I case still exhibited a softer response, as expected, although the maximum response does not seem to reflect this when looking at the maximum response overview.

Figure 3.9(a) depicts a response of SEA-9 in which there was no visible difference between the roof drifts for the base and R-I cases, even when the ground motion ('scmpetr.n45') caused a significant inelastic excursion. A careful inspection of Figure 3.9(b) reveals that there was some noticeable distinction between the first story drifts which confirms that the R-I model indeed showed a softer response in the lower stories where drifts were concentrated. However, the difference in maximum story drift for base and R-I cases was a meager 0.5% and likewise other response histories for SEA-9 also showed no significant effects of residual stresses and initial imperfections. BOS-9 behaved in a manner similar to BOS-3 and its response was again typically characterized by very small drifts and negligible difference in drifts for the base and R-I models (Tables 3.1 and 3.2).

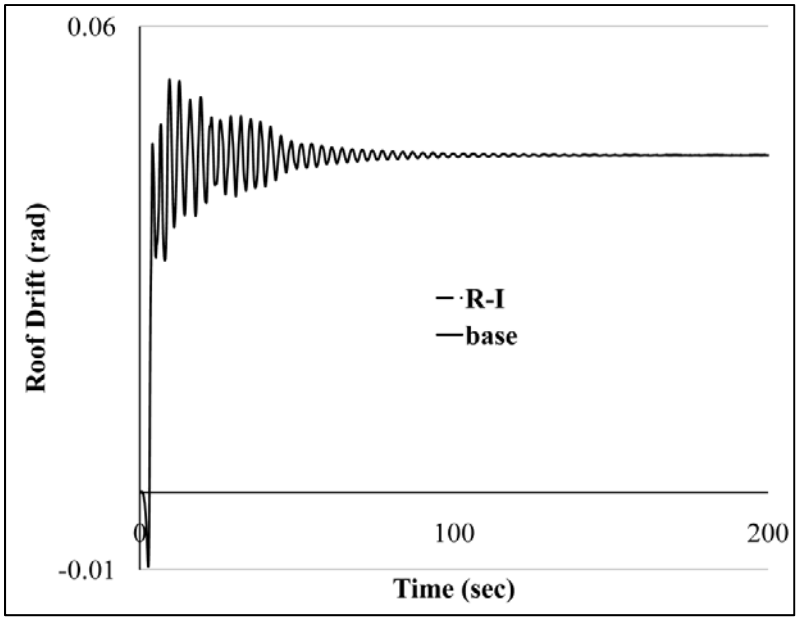

(a)

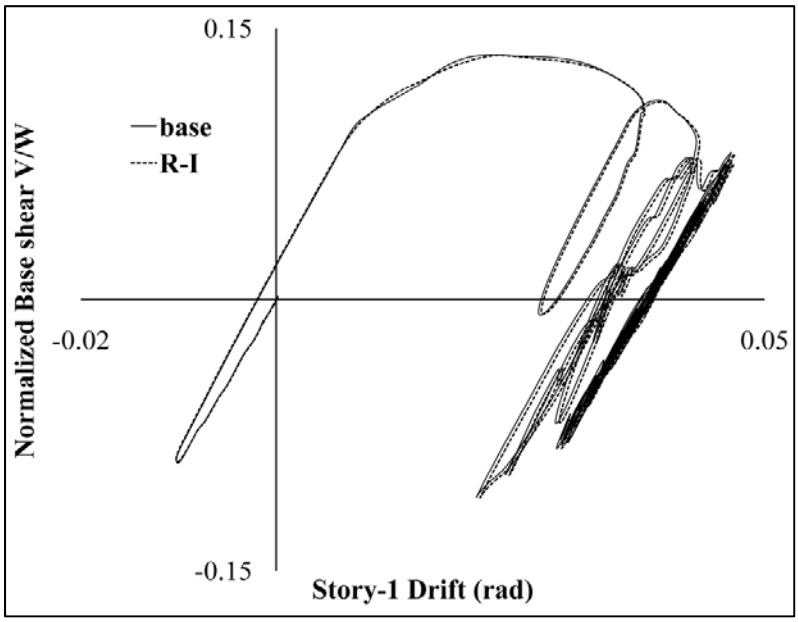

(b)

Figure 3.9 - Response history of SEA-9 for 'scmpetr.n45' record: (a) roof drift vs. time; (b) normalized base shear vs. story-1 drift

3.4.3 Response of 20-Story Frames

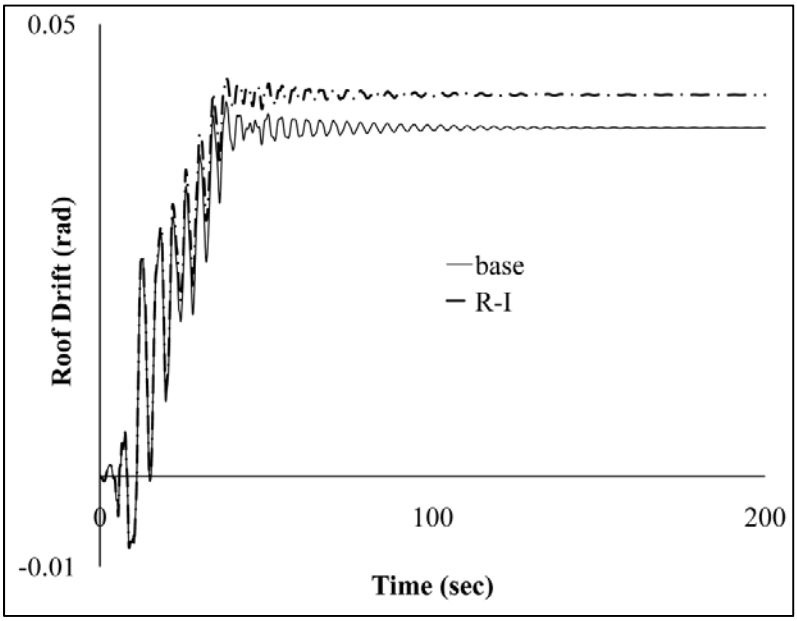

(a)

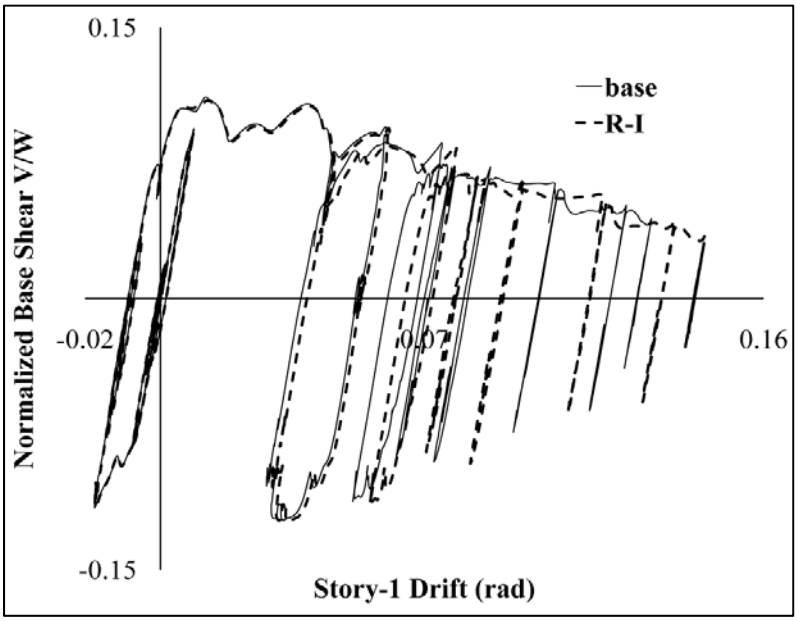

(b)

Figure 3.10 - Response history of LA-20 for 'ltbtab.p45' record: (a) roof drift vs. time; (b) normalized base shear vs. story-1 drift

Figure 3.10 presents one of the severe responses of LA-20 observed under the 'p45' component of a 2/50 ground motion called 'ltbtab' (ltbtab.p45). This ground motion caused a

series of inelastic excursions in LA-20 and led to a 12% difference in both residual roof drift and maximum residual story drift. This difference is clearly visible in Figure 3.10(a). Figure 3.10(b) shows that the difference in base and R-I responses became increasingly evident with each inelastic excursion. Initially the two models behaved identically but their responses became significantly distinct as the R-I model exhibited a softer behavior and led to larger drift concentration in its bottom stories. Figure 3.11 confirms that a soft story mechanism was beginning to form in the lower stories of both models which could potentially lead to collapse under more severe conditions. Such a collapse behavior will be discussed in Chapter 4. Several other LA-20 response histories showed noticeable differences between base and R-I cases but in general the differences were very small, as can been seen Tables 3.1 and 3.2.

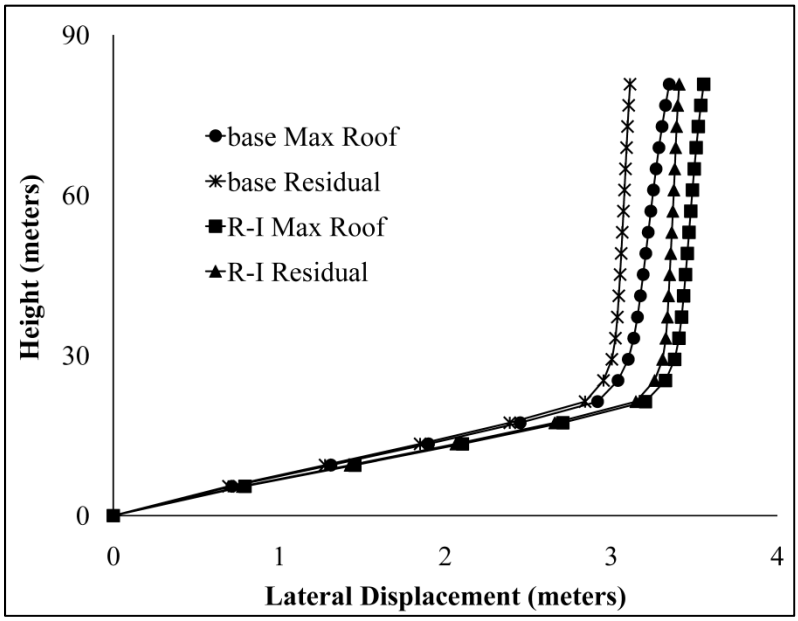

Figure 3.11 - Displacement profiles of LA-20 at maximum roof and residual drifts under 'ltbtab.p45' record

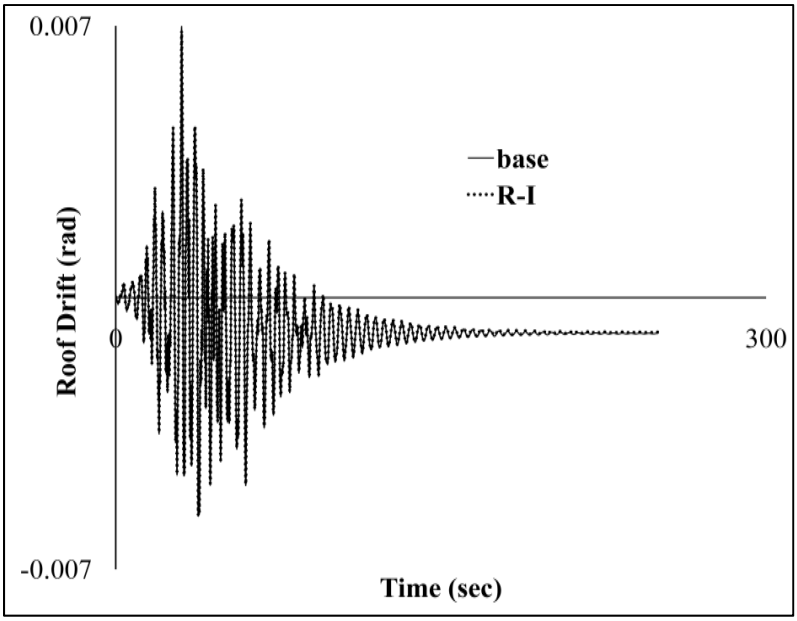

(a)

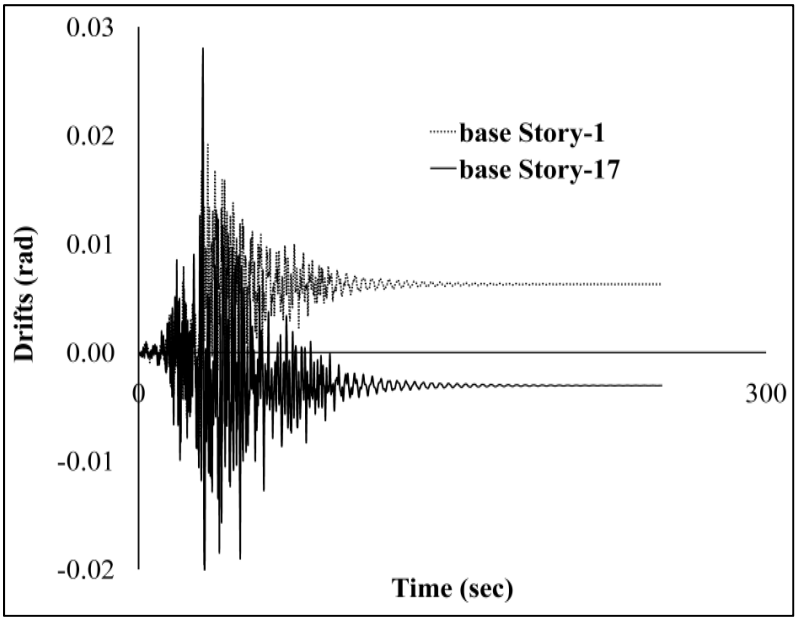

(b)

Figure 3.12 - Response history of SEA-20 for 'svlllol.p45' record: (a) roof drift vs. time; (b) story drift vs. time

Figure 3.12 illustrates a peculiar response history obtained for SEA-20 under the 'p45' component of a 2/50 ground motion called 'svlllol' (svlllol.p45). Similar to the values reported

for SEA-20 in Table 3.1, responses for the base and R-I cases were almost identical for this ground motion (Figure 3.12(a)). However, it is worth noting that the residual roof displacement in Figure 3.12(a) ended up being negative even though the maximum roof drift was in the positive direction. Figure 3.12(b) reveals that the seventeenth story of the baseline model sustained a larger drift than the first story due to effects of higher modes of vibration in the dynamic behavior of the frame. Figure 3.13 shows that at the time of maximum roof displacement, drifts are clearly concentrated in the upper stories. Thus, subsequent negative cycles of the ground motion caused 'ratcheting' in the upper stories whereby the frame incrementally accumulated increasing drift in the negative direction. This resulted in the negative residual roof displacements. It seems that a potential for soft story formation exists in the upper stories and this aspect will be discussed further in Chapter 4.

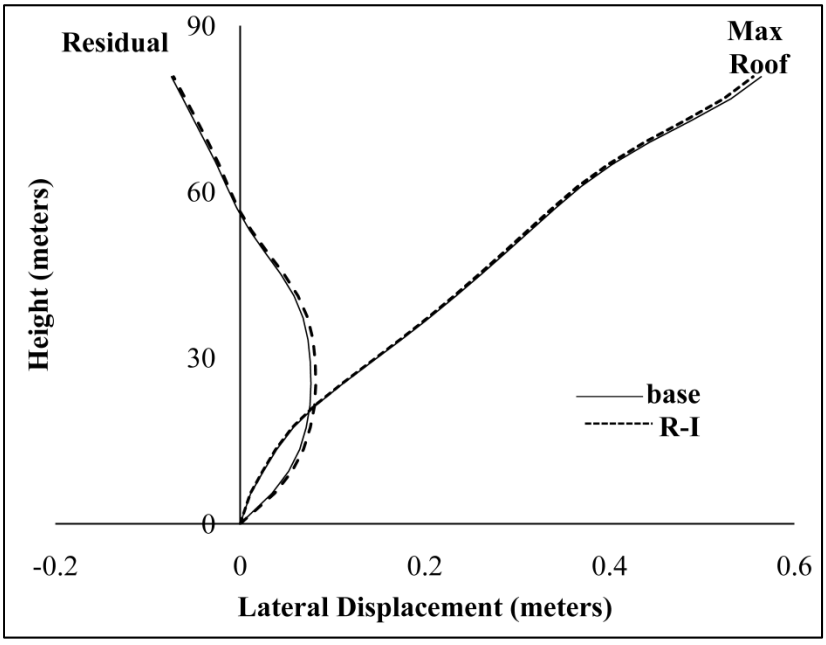

Figure 3.13 - Displacement profiles of SEA-20 at maximum roof and residual drifts under 'svlllol.p45' record

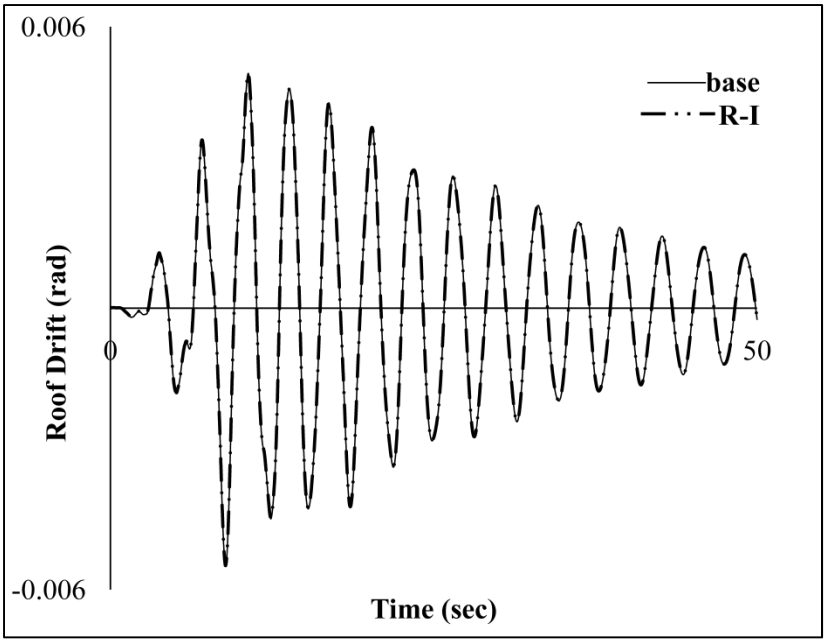

(a)

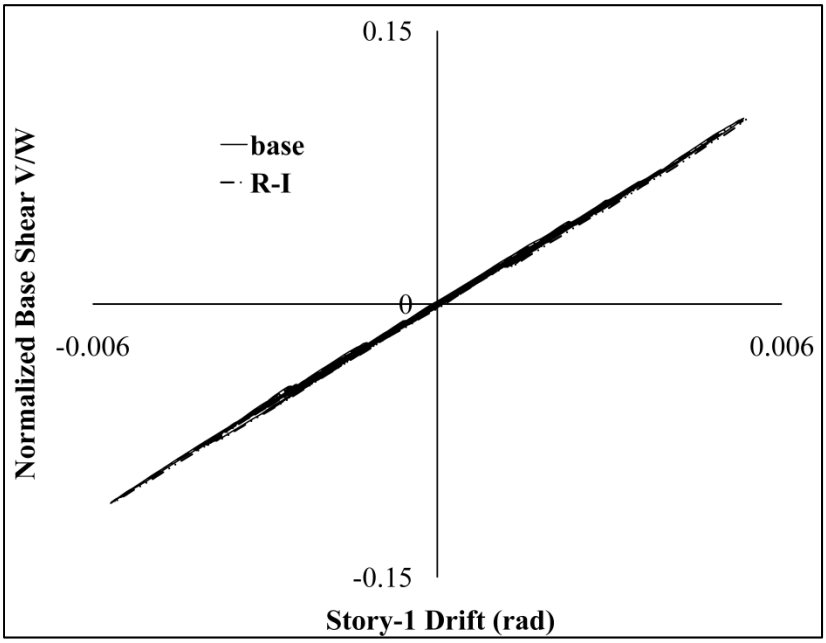

(b)

Figure 3.14 - Response history of BOS-20 for 'bnasta3.n45' record: (a) roof drift vs. time; (b) normalized base shear vs. story-1 drift

Lastly, a typical response history for BOS-20 is shown in Figure 3.14. In Figures 3.14(a) and 3.14(b), roof drift versus time and first story shear versus drift are shown, respectively,

which were obtained under the 'n45' component of a 2/50 ground motion called 'bnasta3' (bnasta3.n45). Similar to BOS-3 and BOS-9, no appreciable difference between the responses of base and R-I cases was observed, as can be seen in Figure 3.14(a). Moreover, Figure 3.14(b) shows that the ground motion caused no inelastic deformations in the frame and the response was also identical in the bottom story. For the Boston frames, the wind loads governed the design and they are much stronger than required for seismic considerations. Hence, these frames remained in the elastic range for almost all ground motions and the drift response was very small.

3.5 Conclusions

The nonlinear static analysis results presented in this chapter indicate that there are no significant differences between the response of frame models that included residual stresses and initial imperfections and those without these effects. Minor differences in cyclic responses were observed even after numerous inelastic cycles that on the surface could appear to nullify the effects of residual stresses and initial imperfections. Although the models with these effects experienced instability slightly earlier, both analysis cases captured the instability triggered by soft story formation and the instabilities occurred within a relatively close range.

The response history results presented in the previous section suggest that the effects of residual stresses and initial imperfections on stability under dynamic loading may not be as important as demonstrated for the scenarios used in developing the DM. However, for cases with severe drift demands and large inelastic excursions, differences are possible in some cases. Since these differences occur at drift levels larger than what is considered in design codes, inclusion of residual stresses and initial imperfections may not be critical for capturing global

stability behavior. The response of the Boston frames was almost completely elastic and the differences between the base and R-I cases were almost unnoticeable.

CHAPTER 4
CONNECTION CYCLIC STRENGTH DEGRADATION

4.1 Background

Results presented in Chapter 3 have shown that residual stresses and initial imperfections do not have a significant impact on cyclic static and dynamic response of steel SMRFs. As discussed in Chapter 2, these frames were represented by centerline numerical models without explicit consideration of panel zones, doubler plates or composite slabs. So far, consistency was maintained with the research that developed the Direct Analysis Method (DM). To develop more realistic models for capturing seismic behavior, an extensive literature review was conducted to identify factors that are critical for seismic stability of buildings. Detailed findings of this literature review have been presented in Appendix C. This demonstrated that strength and stiffness degradation are a significant consideration in the seismic response analysis of a structure when the structure is near the limit state of collapse. Thus, it is important to evaluate the effects of residual stresses and initial imperfections in more detail with numerical models that incorporate these degradation effects

Tests of steel beam-column moment connections have demonstrated strength and stiffness degradation due to local buckling as cyclic demands increase (e.g., Ricles et al 2000) and models have been developed to capture the important aspects of these behavioral characteristics (e.g., Ibarra et al 2005), as discussed in Appendix C. Since stiffness degradation of connections under cyclic loading has a small impact on global behavior of SMRFs and strength degradation of connections has a large impact (FEMA 2000), only strength degradation was considered in this research.

4.2 Modeling Strength Degradation

The Steel02 uniaxial material model in OpenSees was used to simulate the loss of strength at the connections due to inelastic cyclic loading by assigning negative isotropic hardening parameters to the nonlinear beam-column element fiber sections at the ends of all beam members in the prototype frames. Negative isotropic hardening was calibrated to match experimental results from full-scale cyclic tests on ductile welded unreinforced flange (WUF) moment connections (Ricles et. al. 2000). In addition, the post-yield strain hardening coefficient was reduced from 2% to a small value to better approximate the experimental behavior.

Figure 4.1(a) shows representative moment-rotation response for an exterior WUF connection between a W36x150 beam and strong-axis W14x311 column (Ricles et.al. 2000). Figure 4.1(b) illustrates the simulated moment-rotation response obtained using the numerical model in OpenSees. The model does not capture all aspects of behavior, but it does simulate roughly 20% strength degradation after each inelastic cycle. The numerical model achieves lower peak strength and it degrades earlier than the actual connection behavior, but these approximations were deemed to be reasonable for the purposes of the present study. The results are being used to make relative comparisons between behavior with and without connection cyclic degradation and in particular to evaluate the combinatory effect of degradation along with residual stresses and initial imperfections. For this purpose, the chosen connection parameters, which will produce a slightly more flexible and weaker global response than is realistic, are appropriate since they allow for the effects of residual stresses and initial imperfections to be more clearly observed. Selected analyses from the set presented above are evaluated considering degradation.

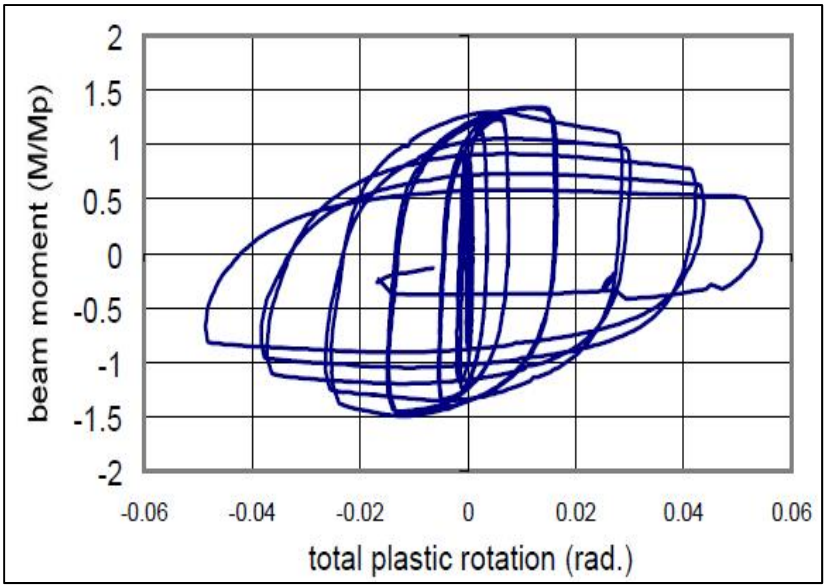

(a)

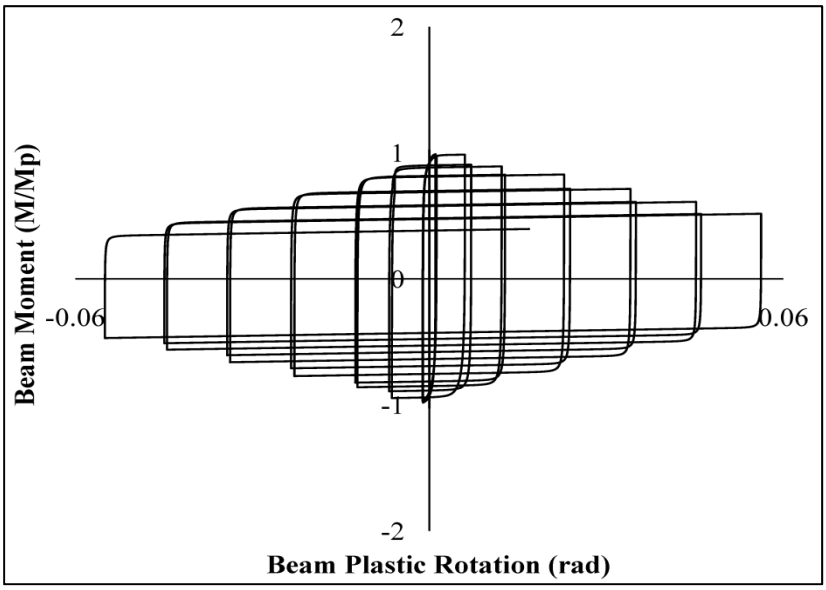

(b)

Figure 4.1 - Connection moment-rotation response: (a) experimental (Ricles et al. 2000); (b) simulated using OpenSees

4.3 Results for Cyclic Pushover Analyses

Figure 4.2 depicts the effect of connection strength degradation on cyclic response of BOS-3 by comparing the base case without degradation (called "base" as before) and with

degradation (called "base-D). Due to the connection strength degradation and the lack of post-yield stiffness, a global negative stiffness is observed. Since yielding at the connections is distributed well over the height of the frame and connection strength degradation is modest, the global lateral capacity is only reduced to 93% of the peak strength after the cycles to 0.03 rad. Figure 4.2 also illustrates the response of the R-I case with degradation (called "R-I-D"). These analyses show that the effects of residual stresses and initial imperfections are very small, like for the frame without connection cyclic strength degradation (Figure 3.3). Cyclic pushover analysis of LA-3 and SEA-3 also produced similar results.

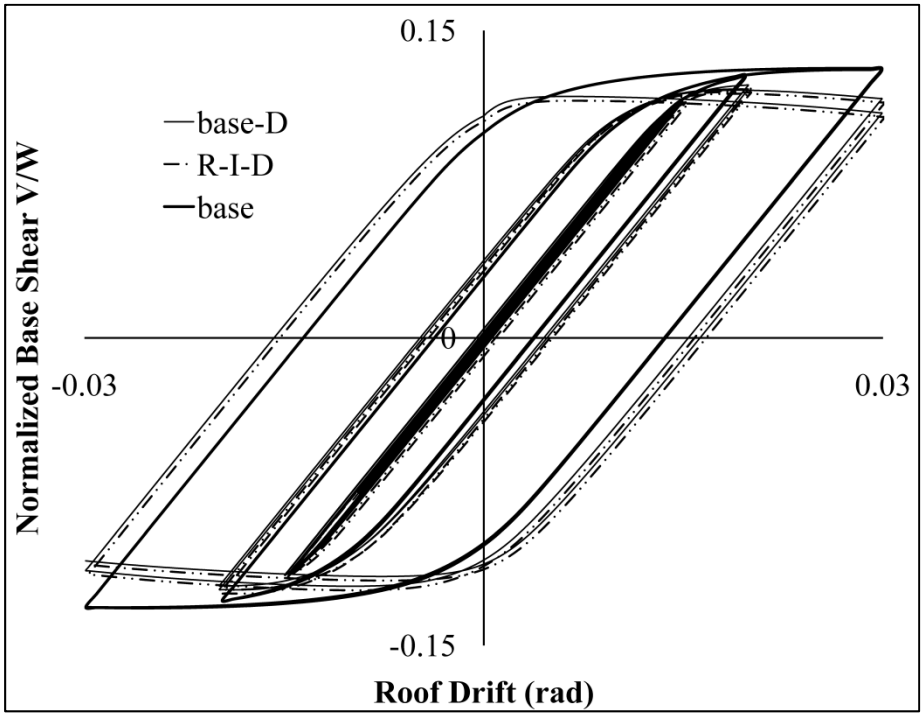

Figure 4.2 - Cyclic pushover response of BOS-3: normalized base shear vs. roof drift

Figure 4.3 depicts the effect of connection strength degradation on cyclic response of BOS-9 by comparing the base and base-D cases. As shown earlier (Figure 3.4), instability was observed in BOS-9, due to concentration of drift in several critical stories toward the bottom of the frame, even when connection cyclic strength degradation was not modeled. Thus, when

connection cyclic strength degradation was incorporated in the numerical model, failure occurred at a slightly earlier stage in the analysis. Figure 4.3 also illustrates the response of the R-I and R-I-D cases. It can be seen that the responses with and without residual stresses and initial imperfections are nearly identical, thus these effects do not exacerbate the effects of strength degradation at the connections. The behaviors of SEA-9 and LA-9 were similar to BOS-3 in the sense that the R-I and base analyses were nearly identical and instability due to soft-story formation was not observed.

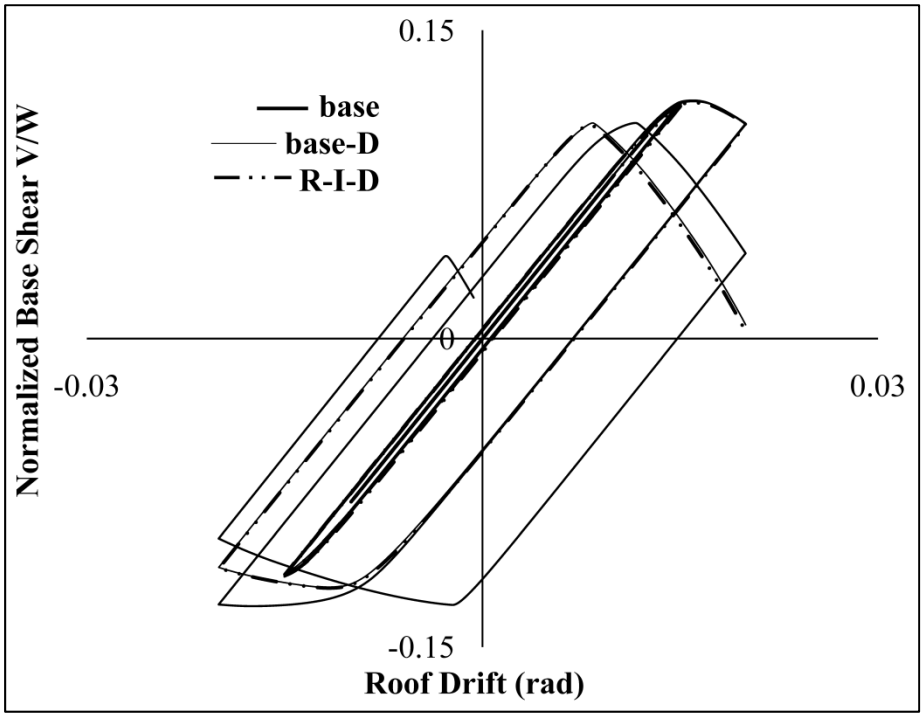

Figure 4.3 - Cyclic pushover response of BOS-9: normalized base shear vs. roof drift

Figure 4.4 shows cyclic response for LA-20 and illustrates the severe effect that connection strength degradation can have. The case without degradation sustained cycles of 0.03 roof drift, whereas the case with degradation was not able to sustain cycles beyond 0.02. Figure 4.4 also compares the base-D and R-I-D cases and it can be seen that the two responses are

nearly identical. Cyclic pushover response for the SEA-20 and BOS-20 was also consistent with this observation.

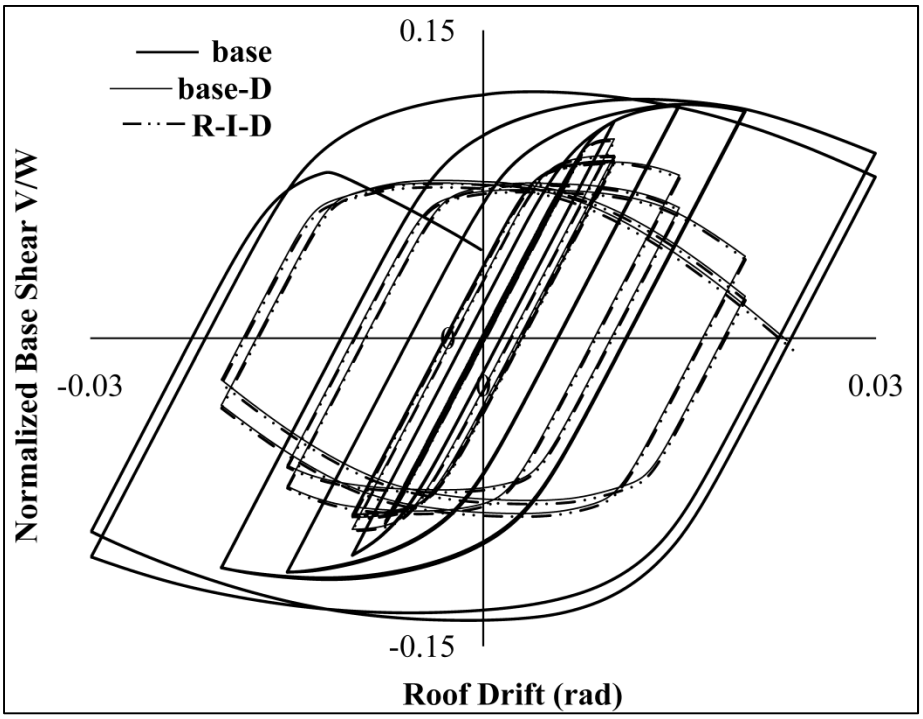

Figure 4.4 - Cyclic pushover response of LA-20: normalized base shear vs. roof drift

4.4 Results for Response History Analyses

This portion of the study evaluates the combined effects of residual stresses, initial imperfections and connection cyclic strength degradation in SMRFs under earthquake loading. For this comparison, the three most severe 2/50 response histories were chosen for each frame based on the full analysis suite where connection cyclic strength degradation was not considered. Table 4.1 summarizes the results for all frames where scenarios with and without degradation were run. As noted previously, the Boston frames are omitted from the following discussion since their response is essentially elastic even under 2/50 records. For this evaluation, a frame was considered to be unstable when the model failed to converge due to roof drift increasing

without bound or when the global roof drift exceeded 0.1 rad. This roof drift limit, although arbitrary, has commonly been used in studies of SMRFs to indicate collapse (FEMA 2000).

Frame	Record	Base		R-I		base-D		R-I-D	
		Roof	Story	Roof	Story	Roof	Story	Roof	Story
LA-3	lpvst03.p45	0.097	0.109	0.098	0.109	C	C	C	C
	lpvst06.n45	0.030	0.033	0.030	0.033	0.032	0.034	0.032	0.035
	lepst13.n45	0.076	0.085	0.077	0.087	0.073	-0.091	0.074	-0.090
SEA-3	svlvina.n45	0.094	0.110	0.100	0.116	C	C	C	C
	scmpetr.n45	0.064	0.078	0.065	0.079	0.072	0.084	0.075	0.084
	sseolym.n45	0.083	0.101	0.089	0.102	C	C	C	C
BOS-3	bnasta3.n45	0.013	0.015	0.013	0.016	0.013	0.016	0.013	0.016
	bsgsm08.n45	0.012	0.029	0.012	0.029	0.012	0.030	0.012	0.030
	bsgsm10.p45	0.009	0.027	0.009	0.027	0.009	0.027	0.009	0.027
LA-9	llplgpc.p45	0.044	0.101	0.045	0.105	C	C	C	C
	lpvst06.p45	-0.031	0.046	-0.030	0.045	-0.025	0.046	-0.024	0.046
	lepst10.p45	-0.029	-0.050	-0.029	-0.048	-0.029	-0.051	-0.028	-0.050
SEA-9	svlllol.n45	0.016	0.027	0.017	0.028	0.022	0.032	0.025	0.035
	scmpetr.n45	0.053	0.067	0.053	0.067	0.076	0.103	0.076	0.103
	smkofun.p45	0.028	0.040	0.028	0.040	0.062	0.065	0.062	0.067
BOS-9	bnasta1.p45	0.010	0.014	0.010	0.014	0.010	0.014	0.010	0.014
	bnasta2.p45	0.006	0.009	0.006	0.009	0.006	0.009	0.006	0.009
	bnasta3.n45	-0.010	0.014	-0.010	0.014	-0.010	0.014	-0.010	0.015
LA-20	lpvst03.p45	0.019	0.066	0.020	0.067	C	C	C	C
	ltbtab.p45	0.041	0.151	0.044	0.167	C	C	C	C
	lepst13.n45	0.036	0.099	0.036	0.100	C	C	C	C
SEA-20	sezerzi.n45	-0.011	0.024	-0.011	0.025	-0.010	0.021	-0.010	0.023
	scmpetr.n45	0.022	0.031	0.022	0.032	0.024	0.036	0.023	0.037
	svlllol.p45	0.007	0.028	0.007	0.028	0.007	0.029	-0.007	0.029
BOS-20	bbns2fw.n45	-0.003	0.004	-0.003	0.004	-0.003	0.004	-0.003	0.004
	bnasta1.p45	-0.006	0.005	-0.006	0.005	-0.006	0.005	-0.006	0.005
	bnasta3.n45	-0.005	-0.006	-0.005	-0.006	-0.005	-0.006	-0.005	-0.006

Table 4.1 - Comparison of maximum drift quantities for response history analyses with and without connection cyclic strength degradation using 2/50 records (C indicates collapse)

4.4.1 Response of 3-Story Frames

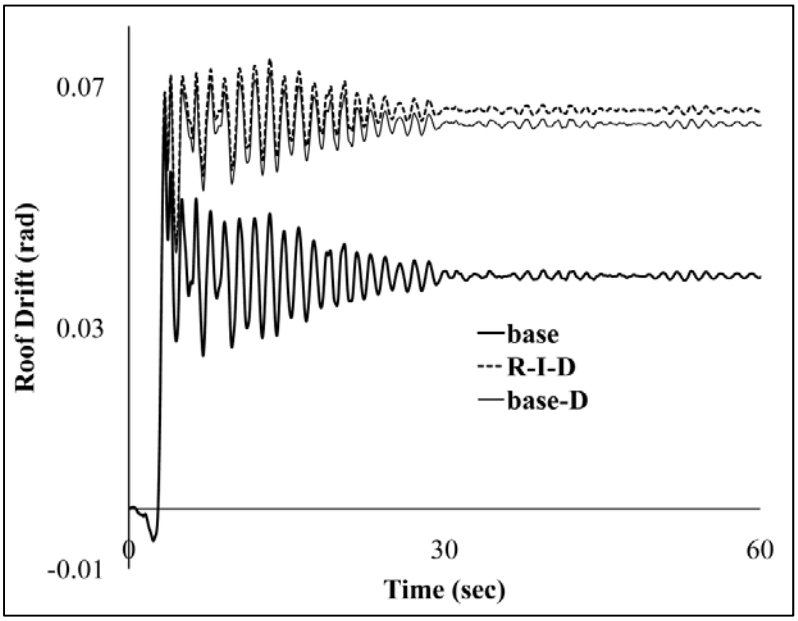

(a)

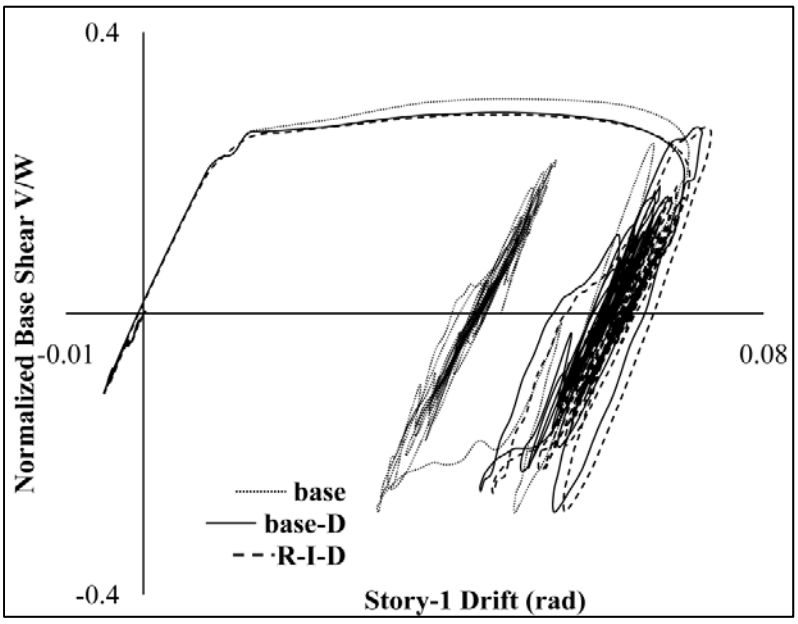

(b)

Figure 4.5 - Response history of SEA-3 for 'scmpetr.n45' record: (a) roof drift vs. time; (b) normalized base shear vs. story-1 drift

Figure 4.5(a) illustrates the impact of residual stresses and initial imperfections compared to degradation by plotting roof drift response histories for SEA-3 for three analysis cases: base,

base-D and R-I-D. For the 2/50 record named scmpetr.n45, the base-D case experienced a maximum roof drift that was 13% larger than the base case. Moreover, residual story drift was found to be 50% greater in the latter case. This confirms that cyclic strength degradation affects the dynamic behavior significantly. In contrast, there is very little difference between the base-D and R-I-D cases. Figure 4.5(b), which plots first story shear vs. drift shows that base-D and R-I-D cases were nearly identical until a large pulse in the positive direction pushed the R-I-D case slightly further inelastically, leading to the subsequent offset in response. However, this difference is very small compared to the change in response due to degradation.

Figure 4.6 depicts the roof drift time history for SEA-3 cases when subjected to the 2/50 record named sseolym.n45. It can be seen that both base-D and R-I-D cases experienced global instability. Table 4.1 shows that even without degradation, SEA-3 exhibited a roof drift larger than 0.08 rad when subjected to the sseolym.n45 record and thus it is expected that the roof drift would be significantly larger when strength degradation is incorporated. Similarly, for the svlvina.n45 record, SEA-3 had roof drift exceeding 0.1 rad for both base-D and R-I-D cases and was judged to have collapsed. The other response histories for LA-3 and SEA-3 showed behavior very similar to the cases discussed above, where the difference between the base-D and R-I-D cases was only slight.

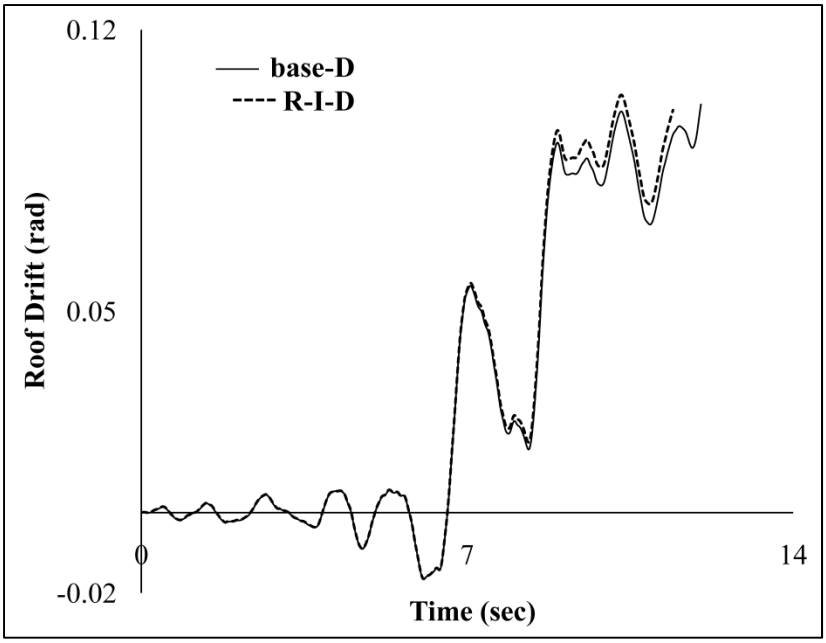

(a)

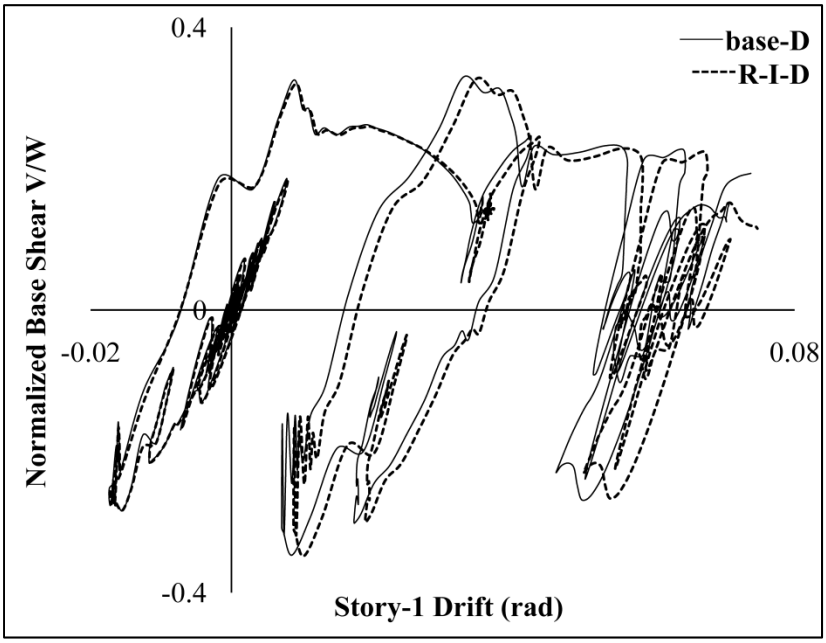

(b)

Figure 4.6 - Response history of SEA-3 for 'sseolym.n45' record: (a) roof drift vs. time; (b) normalized base shear vs. story-1 drift

4.4.2 Response of 9-Story Frames

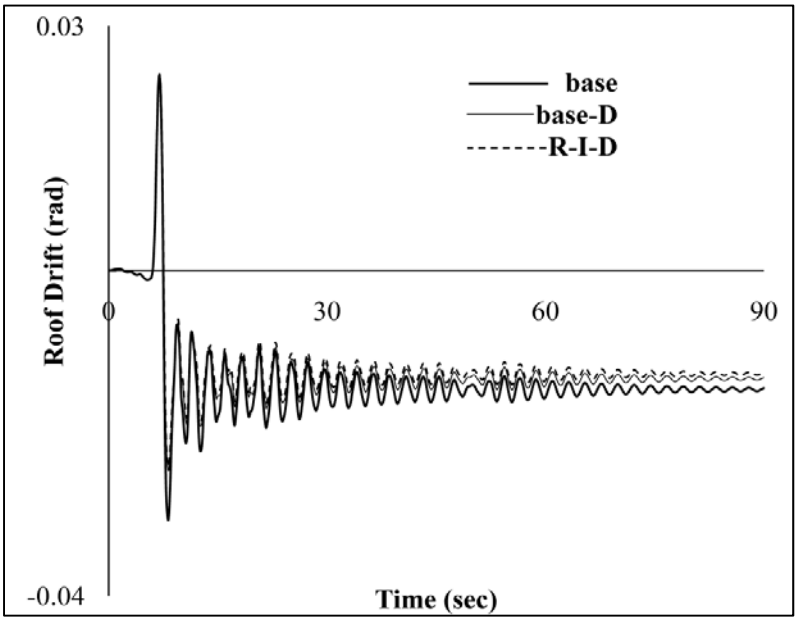

(a)

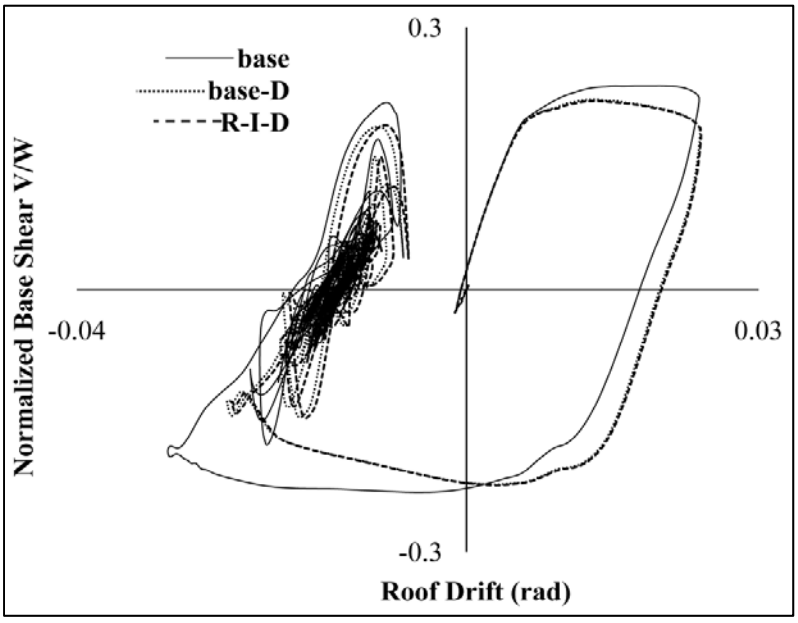

(b)

Figure 4.7 - Response history of LA-9 for 'lpvst06.p45' record: (a) roof drift vs. time; (b) normalized base shear vs. roof drift

Figure 4.7 depicts the response of LA-9 for a record named lpvst06.p45. As can be seen in Table 4.1, it is one of the few scenarios where drifts for the R-I-D case were found to be

smaller than the base-D case. Figure 4.7(a) shows the roof drift response histories for base, base-D and R-I-D cases and it can be seen that roof drift for the R-I-D case is the smallest. Figure 4.7(b) plots base shear vs. roof drift response which clarifies the reason behind the above observation. It can be seen in Figure 4.7(b) that the R-I-D case was pushed farthest inelastically in the positive direction, followed by the base-D case, and thus their responses lagged behind the base case when the loading reversed and the maximum drift for the record was achieved. This behavior is similar to that illustrated in Figure 3.8 and occurs because the base-D and R-I-D models produce a softer response than the base case. Similar observations were made for LA-9 frame under another record named lepst10.p45 (Table 4.1), while the base-D and R-I-D models of LA-9 collapsed when subjected to the record llplgpc.p45.

A typical response of SEA-9 is illustrated in Figure 4.8 where the effect of cyclic strength degradation is highly prominent but there is no difference between the base-D and R-I-D cases. Figure 4.8(a) shows that for the 2/50 record named scmpetr.n45, the base-D case experienced a maximum roof drift that was 44% larger than the base case which implies that degradation had a severe effect on the frame behavior. However, there is almost no difference between the base-D and R-I-D cases. Figure 4.8(b) plots first story shear vs. drift which shows that although the ground motion caused large inelastic excursions, the base-D and R-I-D responses remained nearly identical. This result again highlights that cyclic strength degradation at connections has much greater impact on the seismic response of steel moment-resisting frames than residual stresses and initial imperfections do.

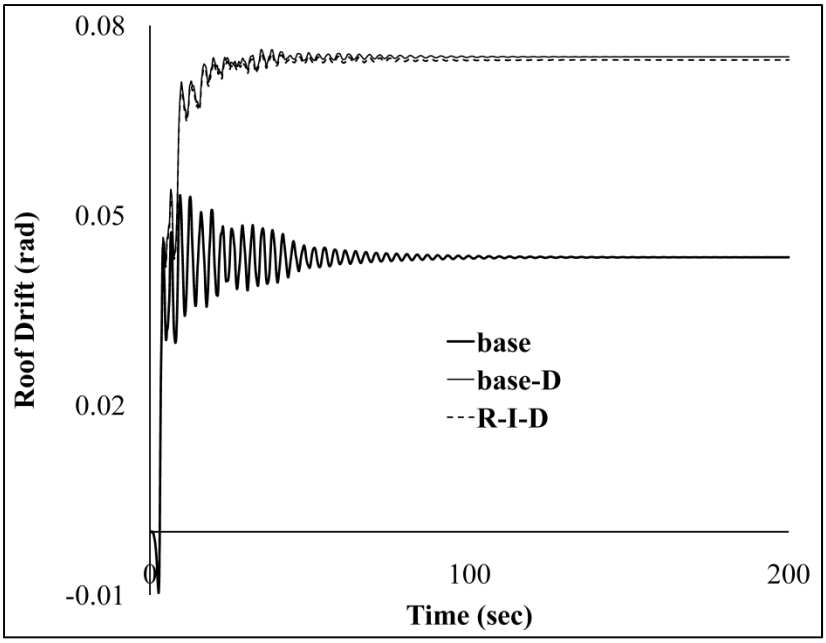

(a)

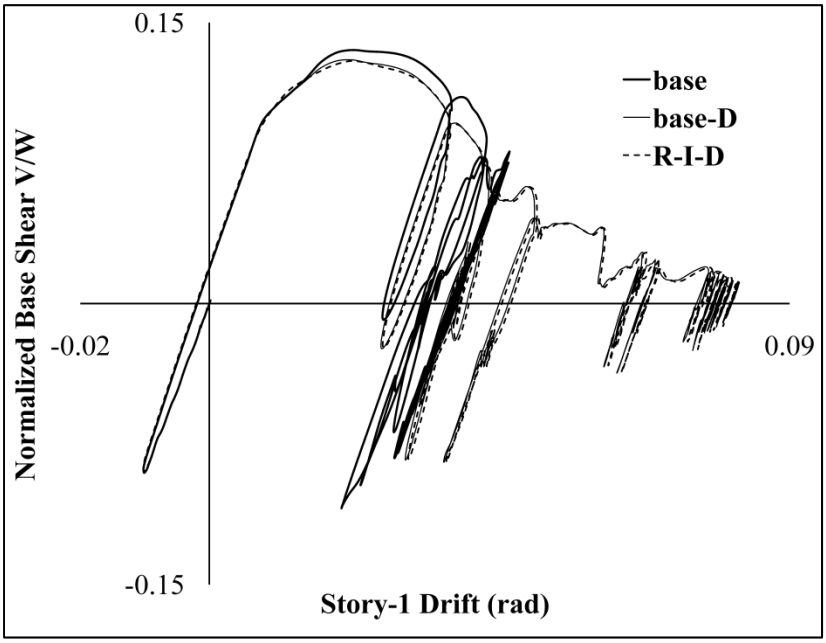

(b)

Figure 4.8 - Response history of SEA-9 for 'scmpetr.n45' record: (a) roof drift vs. time; (b) normalized base shear vs. story-1 drift

4.4.3 Response of 20-Story Frames

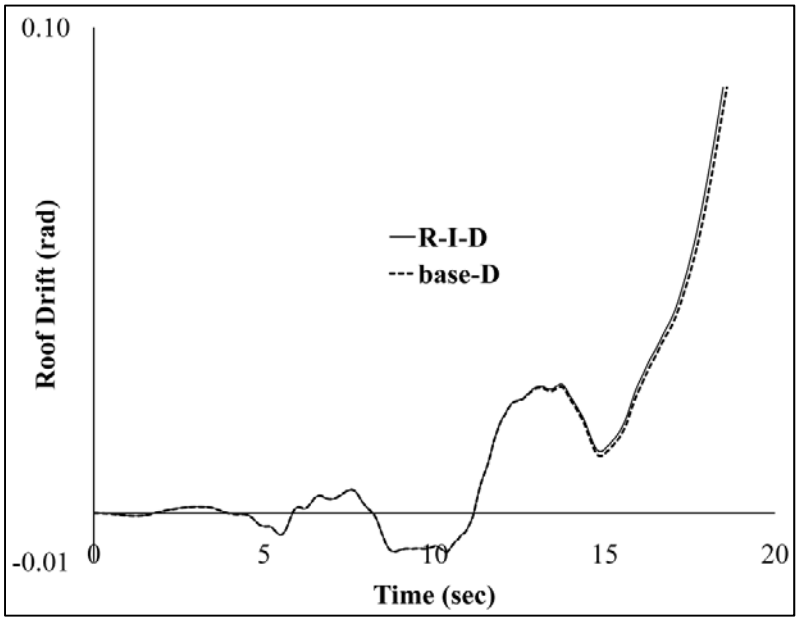

(a)

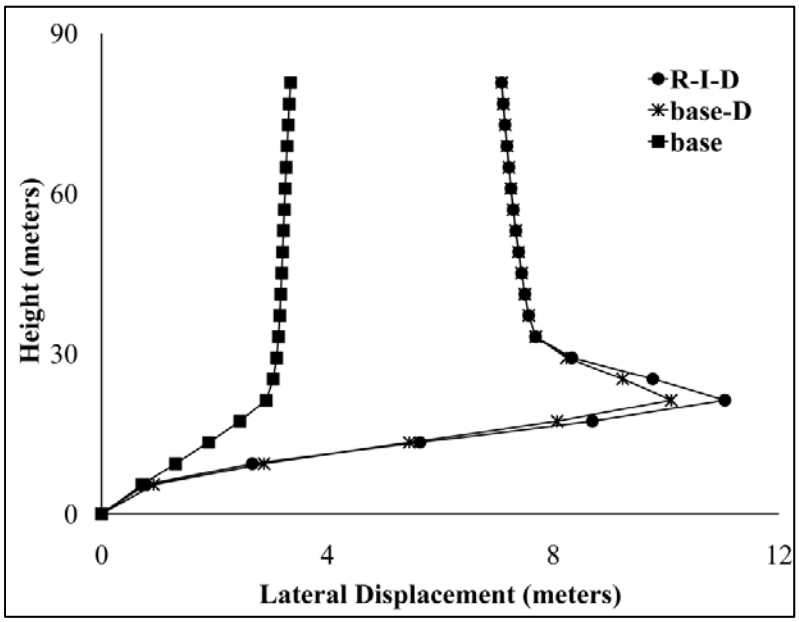

(b)

Figure 4.9 - Response history of LA-20 for 'ltbtab.p45' record: (a) roof drift vs. time; (b) displacement profiles at maximum story drift

LA-20 was deemed to have collapsed for all three of the chosen records when degradation was incorporated. Figure 4.9 illustrates one such case obtained under the record

ltbtab.p45. It can be seen in Figure 4.9(a) that the response of the base-D and R-I-D cases were almost identical, the only difference being that the R-I-D case reached the roof drift level of 0.1 rad slightly earlier. Figure 4.9(b) compares the displacement profiles at maximum story drift for the two models with the base case and confirms that a soft story mechanism developed in the lower stories, as expected based on the discussion in Chapter 3 (Figures 3.10 and 3.11). The maximum story displacement for the R-I-D case was found to be 10% larger than the base-D case and nearly three times the base case. However, it is interesting to note that for the three chosen records for LA-20 no scenario was found in which the base-D case was stable while the R-I-D case was unstable.

SEA-20 showed behavior similar to SEA-3 whereby incorporating degradation did not magnify the impact of residual stresses and initial imperfections. Figure 4.10 depicts the response of SEA-20 under a record named svlllol.p45. As discussed previously in Chapter 3 (Figures 3.12 and 3.13), drift concentration in upper stories and subsequent ratcheting led to the peculiar response in which maximum roof drift was positive while the residual roof drift ended up being negative (Figure 4.10(a)). In addition, Table 4.1 shows that the maximum roof drift for the R-I-D case was found to be negative while the maximum story drift remained positive. Careful inspection of Figure 4.10(a) shows that the base-D case attained maximum roof drift at t = 25 seconds, while the R-I-D case attained its maximum roof drift at t = 60 seconds. Thus, it is evident that the R-I-D roof drift reached its maximum value after ratcheting had begun and the frame started drifting only in the negative direction. However, Figure 4.10(b) shows that both base-D and R-I-D models achieved a positive maximum story drift in story-17 at t = 25 seconds.

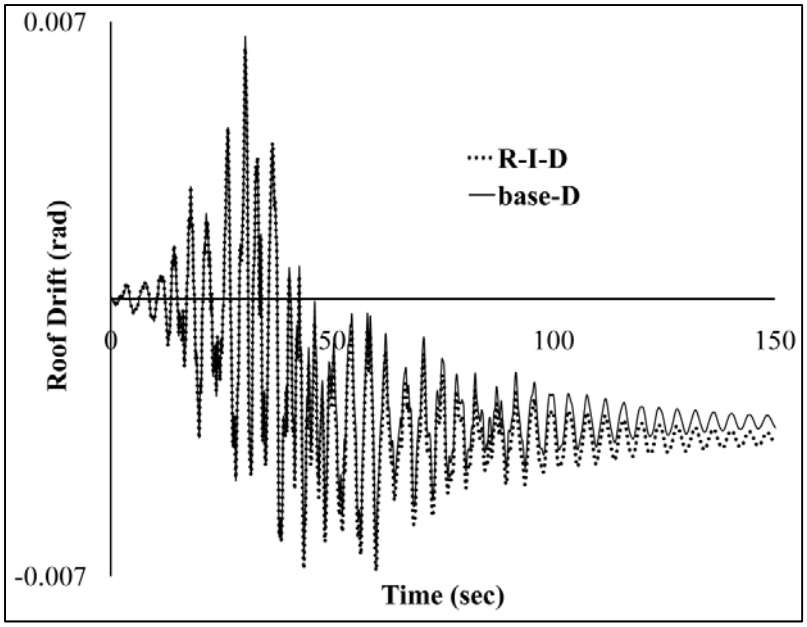

(a)

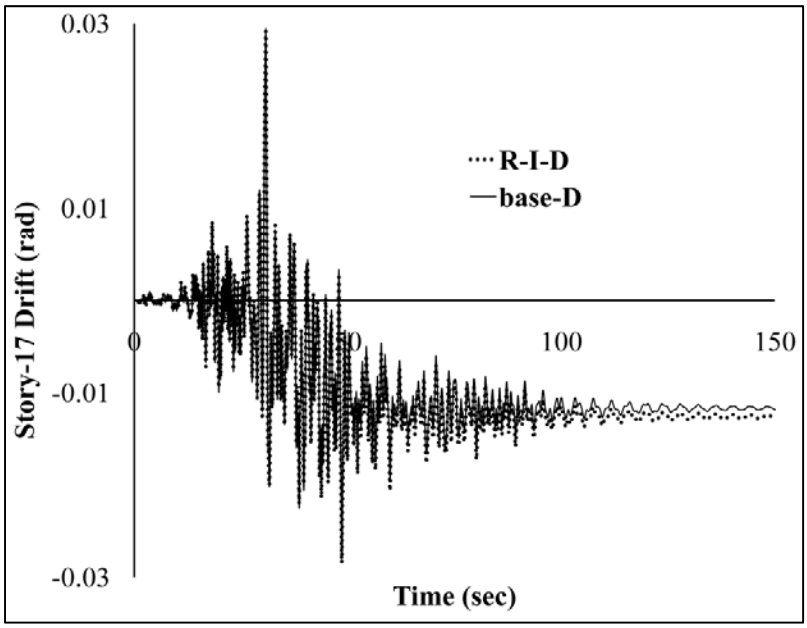

(b)

Figure 4.10 - Response history of SEA-20 for 'svlllol.p45' record: (a) roof drift vs. time; (b) story drift vs. time

Figure 4.11 confirms this observation by showing that the displacement profiles for the two models were nearly identical when maximum story drift was achieved. However, the two models

attained maximum roof drift in opposite directions because the softer R-I-D model underwent higher roof displacements after the onset of ratcheting.

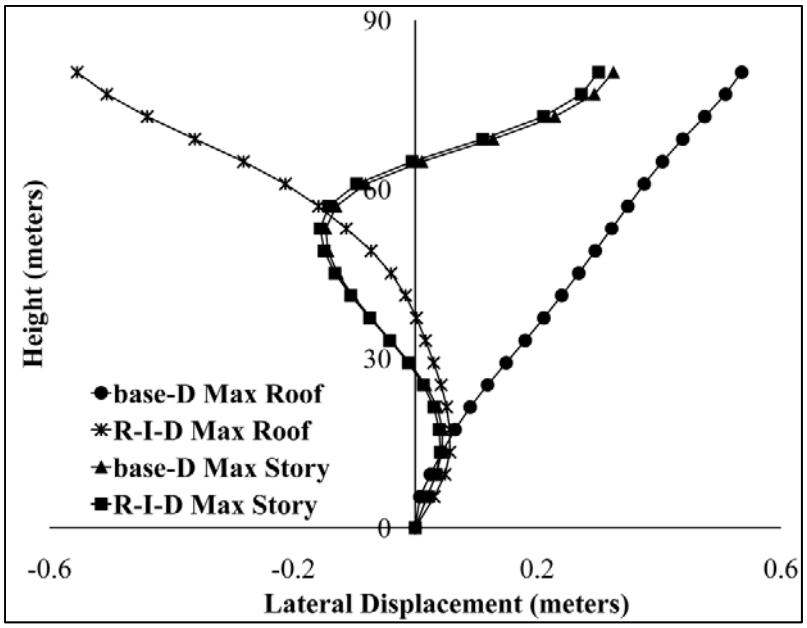

Figure 4.11 - Displacement profiles of SEA-20 at maximum roof and story drift under 'svlllol.p45' record

4.5 Conclusions

The results presented for cyclic pushover analysis of frame models with degradation characteristics yielded the same result in general: connection cyclic strength degradation can cause collapse in some cases, but the effects of residual stresses and initial imperfections are almost imperceptible when connection cyclic strength degradation is modeled.

From the results for response history analysis discussed in this chapter, it is evident that even when the worst-case frame behavior was considered, the impact of residual stresses and initial imperfections did not prove to be a critical factor in seismic stability of the chosen steel moment-resisting frames. Even for frames that showed unstable behavior, residual stresses and initial imperfections only slightly hastened the process of collapse. However, no scenario was

found in which a case without residual stresses and initial imperfections was stable and the case with these effects was unstable. It is clear that cyclic strength degradation has far more impact on the seismic stability behavior of steel moment-resisting frames than residual stresses and initial imperfections do.

CHAPTER 5
IMPLICATIONS AND CONCLUSIONS

5.1 Design Implications

To link the analysis results in this study more tangibly to the design process, sample axial-flexural (*P-M*) interaction checks for selected members in LA-9 were conducted. The *ASCE-7* load combination of $1.2D + 0.5L + 1.0E$ was chosen for this purpose. It is important to note that this frame was originally designed per the provisions of the 1994 *Uniform Building Code* as described by Gupta and Krawinkler (1999). Thus, earthquake loads were calculated accordingly, taking into account the differences between the Allowable Stress Design (ASD) and Load and Resistance Factor Design (LRFD) approaches, to ensure that a representative LRFD load case was used for the interaction checks. The detailed load calculation has been shown in Appendix D. Table 5.1 presents the interaction values for the first story columns in LA-9, obtained by three different analyses in SAP2000 (CSI 2009), since this is a typical software package used in design offices. Note that the moment-resisting frame beams are pinned at Column A since this column is part of a SMRF in the orthogonal direction. Thus, it has low interaction values for the frame being considered. The three analysis cases were:

(1) A first-order elastic analysis with no stiffness reduction and $K = 1$.

(2) The ELM, in which $K = 1$ since the ratio of second-order drift to first-order drift was less than 1.1. Thus, this analysis was effectively a second-order elastic analysis with $K = 1$.

(3) The DM, which consisted of a second-order elastic analysis with stiffness reduction, but notional loads were not required in addition to the lateral earthquake loads since the ratio of second order drift to first order drift was less than 1.5. As always for the DM, $K = 1$.

Column line	Member	Analysis		
		1st-order elastic analysis no stiffness reduction (K = 1)	ELM (K=1)	DM (K=1)
A	W14x370	0.041	0.040	0.040
B	W14x500	0.27	0.30	0.31
C	W14x500	0.27	0.30	0.31
D	W14x500	0.25	0.28	0.29
E	W14x500	0.25	0.28	0.28
F	W14x370	0.25	0.28	0.29

Table 5.1 - Design axial-flexural interaction values for first-story columns in LA-9

Thus, the comparison of (1) and (2) illustrates the impact of second-order effects (first-order vs. second-order analysis) and the comparison of (2) and (3) illustrates the impact of inelasticity and residual stresses (no stiffness reduction vs. stiffness reduction). The interaction values shown in Table 5.1 indicate that second-order effects and stiffness reduction have little bearing on the design of these members. Second-order effects have a slightly greater effect on the interaction values than stiffness reduction, but this difference is not of practical importance since the total impact of these two parameters is negligible. This finding is consistent with the nonlinear analysis results presented above and supports the broad conclusion that there appears to be no basis for requiring the DM to design ductile steel structures in high seismic regions.

Figure 5.1 highlights the difference between scenarios where the DM captures critical stability-related behavior and cases where the DM does not provide benefit. Figure 5.1(a) depicts three analyses of a one-bay one-story frame originally presented by LeMessurier (1977) as Example 3, which has ultimate strength that is very close to the factored design load. The fraction of design load is plotted against story drift for the same three analysis cases previously presented by White et al. (2006). An extended version of the DM, called the DM-EP since it

uses elastic-plastic hinges in the frame elements, reasonably captures the ultimate strength obtained using distributed plasticity analysis with residual stresses and initial imperfections, while the ELM underestimates drift at the design load level and does not capture post-peak behavior. In contrast, Figure 5.1(b) depicts the response of the first story of LA-9 from distributed plasticity analysis with residual stresses and initial imperfections. The code-prescribed design base shear for this frame is much smaller than the ultimate strength due to stringent drift limitations and the significant overstrength that is typical for SMRFs in high seismic regions. At the design force level, the minor variations in force and deformation demands that arise from different analysis methods have little relevance to the actual behavior of the frame at the ultimate strength level. Although the DM provides a good approximation of the actual behavior for designs governed by non-seismic considerations, such as the LeMessurier Example 3 frame, for seismic design there appears to be no additional benefit or rational basis for using the DM. Further, in ductile steel earthquake-resisting systems (like SMRFs), a simple first-order elastic analysis with $K = 1$ for column strength calculations is adequate for design purposes since this analysis type produces demands that are very similar to those obtained using the DM. The proportioning of such frames is primarily governed by seismic drift limits and thus due to their high lateral stiffness, second-order effects and stiffness reduction have insignificant impact at the design force level. These systems depend on significant ductility to achieve good seismic performance, and expending extra effort to slightly modify design-level demands, such as through the DM, is not justified.

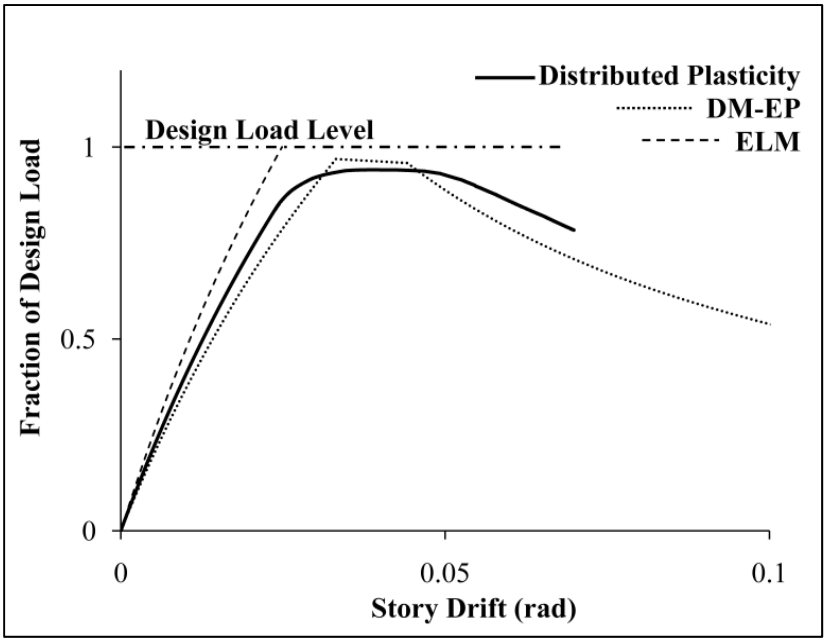

(a)

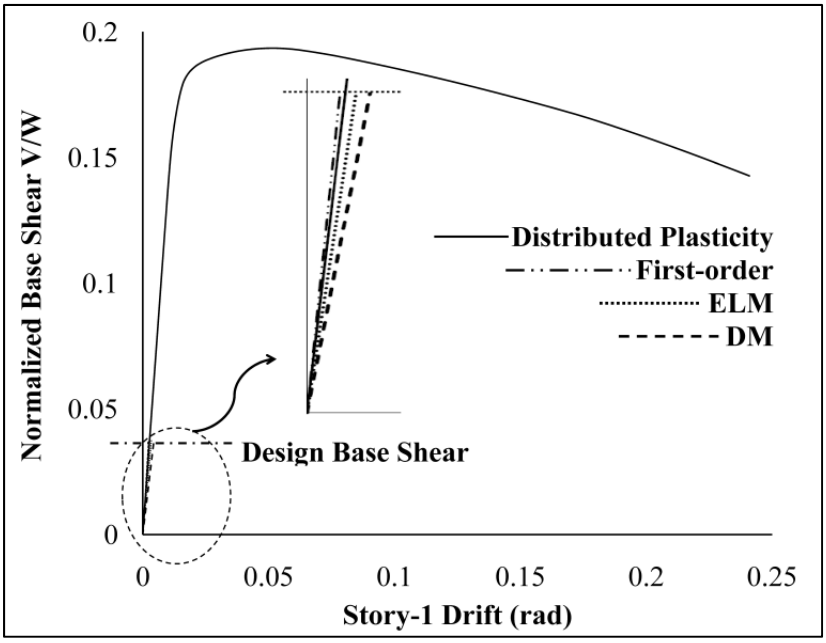

(b)

Figure 5.1 - Contrasting applications of the DM: (a) design governed by non-seismic considerations; (b) typical behavior of a ductile earthquake-resisting system (LA-9)

5.2 Conclusions

The research described in this thesis evaluated the relevance of using the AISC Direct Analysis Method for seismic steel design. For this purpose, 3, 9 and 20-story special steel moment-resisting frames in three different seismic regions were studied. Four models were considered for all nine frames by including or not including (a) residual stresses and initial imperfections and (b) cyclic strength degradation at the beam-to-column connections. Each model was subjected to monotonic pushover analysis, cyclic pushover analysis, and a series of time history analyses. All analyses incorporated material and geometric nonlinearity. The primary findings of this study are:

- No significant differences in the nonlinear static or dynamic responses were observed between frame models that included residual stresses and initial imperfections and those without these effects.
- In scenarios where instability was observed, it occurred in both the models with and without residual stresses and initial imperfections, and the only effect of residual stresses and initial imperfections was to cause the instability to occur slightly earlier.
- When severe cyclic strength degradation was explicitly incorporated in the frame models at the beam-to-column connections, there were no cases where instability occurred in the model with residual stresses and initial imperfections while the model without residual stresses and initial imperfections showed a stable response. This suggests that the effects of residual stresses and initial imperfections do not exacerbate the effect that cyclic strength degradation has on seismic stability.
- Cyclic strength degradation at connections has much greater impact on the seismic stability behavior of steel moment-resisting frames than residual stresses and initial imperfections do.

- Axial-flexural interaction checks at design-level forces showed very little variation between calculations based on first-order elastic analysis with no stiffness reduction and second-order elastic analysis with stiffness reduction.

5.3 Final Remarks

The findings of this study indicate that there is no basis for requiring the Direct Analysis Method (DM) prescribed in the 2010 AISC *Specification* when designing ductile steel earthquake-resisting systems (like SMRFs). For such systems, it is recommended that simple first-order elastic analysis with no stiffness reduction be permitted and that an effective length factor equal to one be used in calculating column strength.

The present study focused only on a particular class of steel frames, namely SMRFs, which generally exhibit a ductile behavior and a high level of system overstrength. Although the seismic behavior of SMRFs contrasted well with the typical scenarios used to develop the DM, studies across a wider range of system parameters would be worthwhile. Other types of steel frames, like intermediate or ordinary moment frames, and industrial/metal building systems should be evaluated in a manner similar to this study. This would help to better understand the usefulness of the DM in the context of seismic design. Moreover, for the DM to be extended to seismic design, consistency must be achieved between the DM and the *ASCE-7* seismic stability design requirements.

REFERENCES

American Institute of Steel Construction. (2010a). *Specification for Structural Steel Buildings.* ANSI/AISC Standard 360-10. AISC, Chicago, Illinois.

American Institute of Steel Construction. (2010b). *Seismic Provisions for Structural Steel Buildings*. ANSI/AISC Standard 341-10. AISC, Chicago, Illinois.

American Institute of Steel Construction. (2010c). *Code of Practice for Steel Buildings and Bridges*. AISC Standard 303-10. AISC, Chicago, Illinois.

American Society of Civil Engineers. (2010). *Minimum Design Loads for Buildings and Other Structures*. ASCE/SEI 7-10. ASCE, Reston, Virginia.

Bridge, R.Q. (1998). "The Inclusion of Imperfections in Probability-Based Limit States Design". *Proceedings, 1998 Structural Engineering World Congress*, San Francisco, California, July.

Computers and Structures, Inc. (CSI), (2009). *Basic Analysis Reference Manual*.

Federal Emergency Management Agency (2000). *State of the Art Report on Systems Performance of Steel Moment Resisting Frames Subject to Earthquake Ground Shaking*, FEMA 355C.

Filippou, F. C., Popov, E. P., Bertero, V. V. (1983). "Effects of Bond Deterioration on Hysteretic Behavior of Reinforced Concrete Joints". *Report EERC 83-19*, Earthquake Engineering Research Center, University of California, Berkeley.

Galambos TV and Ketter RL. (1959). "Columns under combined bending and thrust." *Journal of the Engineering Mechanics Division*. ASCE, 85(EM2), 135-152.

Gupta A and Krawinkler H. (1999). “Prediction of seismic demands for SMRFs with ductile connections and elements.” *SAC Background Document, Report No. SAC-BD-99/06*.

Ibarra, L.F., Medina, R.A. and Krawinkler, H. (2005). “Hysteretic models that incorporate strength and stiffness deterioration.” *Earthquake Engineering and Structural Dynamics*, 34: 1489-1511.

Kim, S. E. (1996). “Practical Advanced Analysis for Steel Frame Design.” Ph.D. Thesis, Purdue University, West Lafayette, IN.

LeMessurier, W.J. (1977). “A Practical Method of Second Order Analysis. Part 2: Rigid Frames.” *Engineering Journal*, AISC, 13(4): 89-96.

Lamarche CP and Tremblay R. (2008). “Accounting for residual stresses in the seismic stability of nonlinear beam-column elements with cross-section fiber discretization.” *2008 Annual Stability Conference*, Structural Stability Research Council, April 2-5, 2008, Nashville, Tennessee, 59-77.

Lee K. and Foutch D.A. (2000). “Performance Prediction and Evaluation of Steel Special Moment Frames for Seismic Loads.” *SAC Background Document, Report No. SAC-BD-00/25*.

Liew, R.J.Y., White, D.W. and Chen, W.F. (1994). “Notional-Load Plastic-Hinge Method for Frame Design.” *Journal of Structural Engineering*, ASCE, 120(5): 1434-1454.

Lu, A.Y.C., MacRae, G.A., Ziemian, R.D., Hann, C., Peng, B.H.H., and Clifton, G.C. (2009). "Extended Direct Analysis of Steel Frames." *SESOC Journal*, 122(2), 89-102.

Maleck A. E. and White D. W. (2000). “Analysis and Design Methods for Partially-Restrained Steel Framing Systems.” *Proceedings, Annual Technical Session, Structural Stability Research Council*, Memphis, July.

Maleck, A. E. (2001). ‘‘Second-order inelastic and modified elastic analysis and design evaluation of planar steel frames.’’ PhD Thesis, Georgia Institute of Technology, Atlanta, GA.

Mazzoni S, McKenna F, and Fenves GL. (2009). *Open System for Earthquake Engineering Simulation User Command-Language Manual*. Pacific Earthquake Engineering Research Center, University of California, Berkeley, Berkeley, California, <http://

OpenSEES.berkeley.edu/OpenSEES/manuals/usermanual/index.html>.

Menegotto, M. and Pinto, P.E.: (1973). “Method of analysis of cyclically loaded RC plane frames including changes in geometry and non-elastic behavior of elements under normal force and bending.” *Preliminary Report*, IABSE, Vol. 13, pp. 15–22.

Okazaki, T., Fahnestock, L.A. and Parkolap, M.J. (2010). “On the Interface of Stability and Seismic Design Requirements for Steel Buildings”. *Proceedings, SSRC Annual Structural Stability Conference*, Orlando, Florida, May 12-15.

Ricles, J. M., Mao, C., Lu, L-W., and Fisher, J. W. (2000). ‘‘Development and Evaluation of Improved Details for Ductile Welded Unreinforced Flange Connections.’’ *ATLSS Rep. No. 00-04*, *SAC Task 7.05*, SAC Joint Venture, Richmond, California.

Salmon, C.G., Johnson, J.E., Malhas, F.A. (2008). ‘‘Steel Structures: Design and Behavior.’’ 5th ed. Prentice Hall, New York.

Somerville, P., et al. (1997). ‘‘Development of ground motion time histories for phase 2 of the FEMA/SAC steel project’’ *Rep. No. SAC/BD-97/04*, SAC Joint Venture, Sacramento, California.

SSRC (1976). “Guide to Stability Design Criteria for Metal Structures”. 3rd Edition. B.G. Johnston (ed.). Structural Stability Research Council, Wiley.

Surovek-Maleck, A.E. and White, D.W. (2004a). “Alternative Approaches for Elastic Analysis and Design of Steel Frames. I: Overview.” *Journal of Structural Engineering*, ASCE, 130(8): 1186-1196.

Surovek-Maleck, A.E. and White, D.W. (2004b). “Alternative Approaches for Elastic Analysis and Design of Steel Frames. II: Verification Studies.” *Journal of Structural Engineering*, ASCE, 130(8): 1197-1205.

White, D.W. and Hajjar, J.F. (1997). “Design of steel frames without consideration of effective length.” *Engineering Structures*, 19(10): 797-810.

White, D.W. and Hajjar, J.F. (2000). “Accuracty and simplicity of alternative procedures for stability design of steel frames.” *Journal of Constructional Steel Research*, 42(2): 209-261.

White, D. W. and Nukala, P. K. V. N. (1997). “Recent Advances in Methods for Inelastic Frames Analysis: Implications for Design and a Look Toward the Future,” *Proceedings, National Steel Construction Conference*, AISC, 43: 1-24.

White D.W., Surovek A.E., Alemdar B.N., Chang C.J., Kim Y.D., and Kuchenbecker G.H. (2006). “Stability analysis and design of steel building frames using the 2005 AISC Specification.” *International Journal of Steel Structures, Korean Society of Steel Construction*, 6, 71-91.

APPENDIX A

BUILDING FRAME LAYOUTS

The figures shown here were originally presented by Dr. T. Okazaki in an unpublished internal report (November 2008).

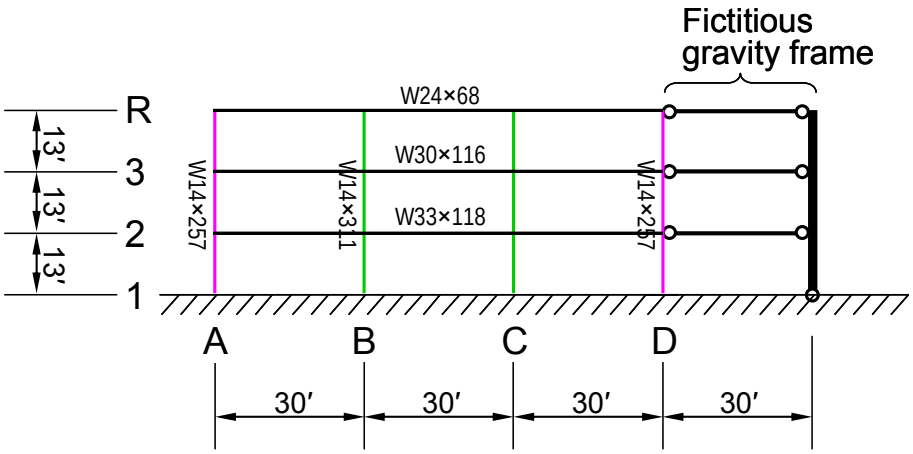

Figure A.1 – Los Angeles 3-Story Frame

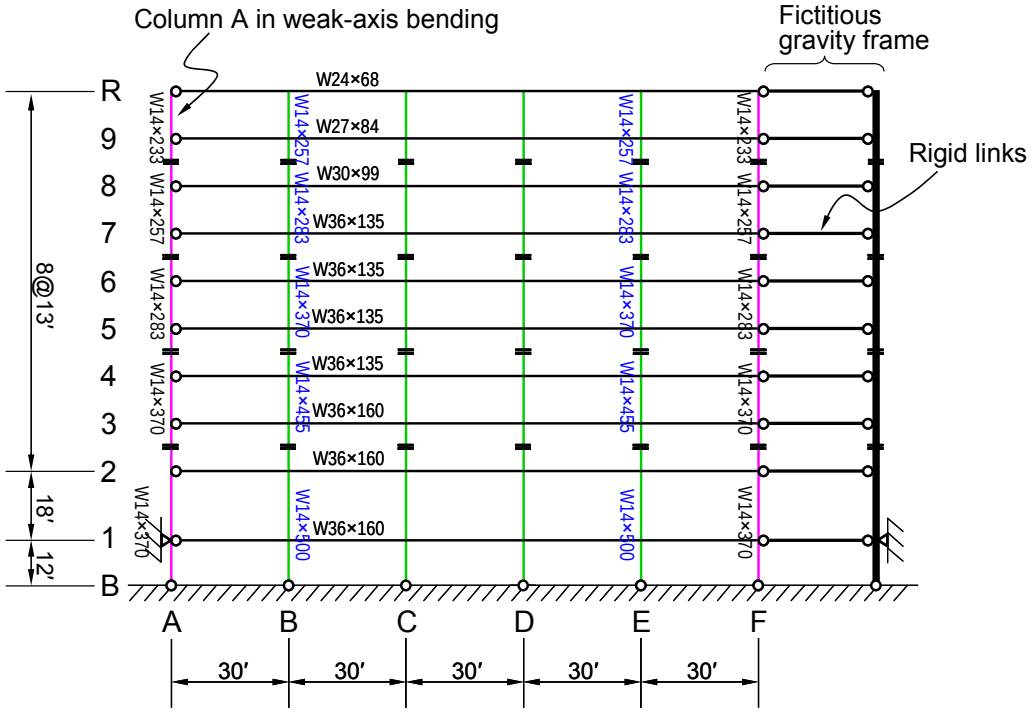

Figure A.2 – Los Angeles 9-Story Frame

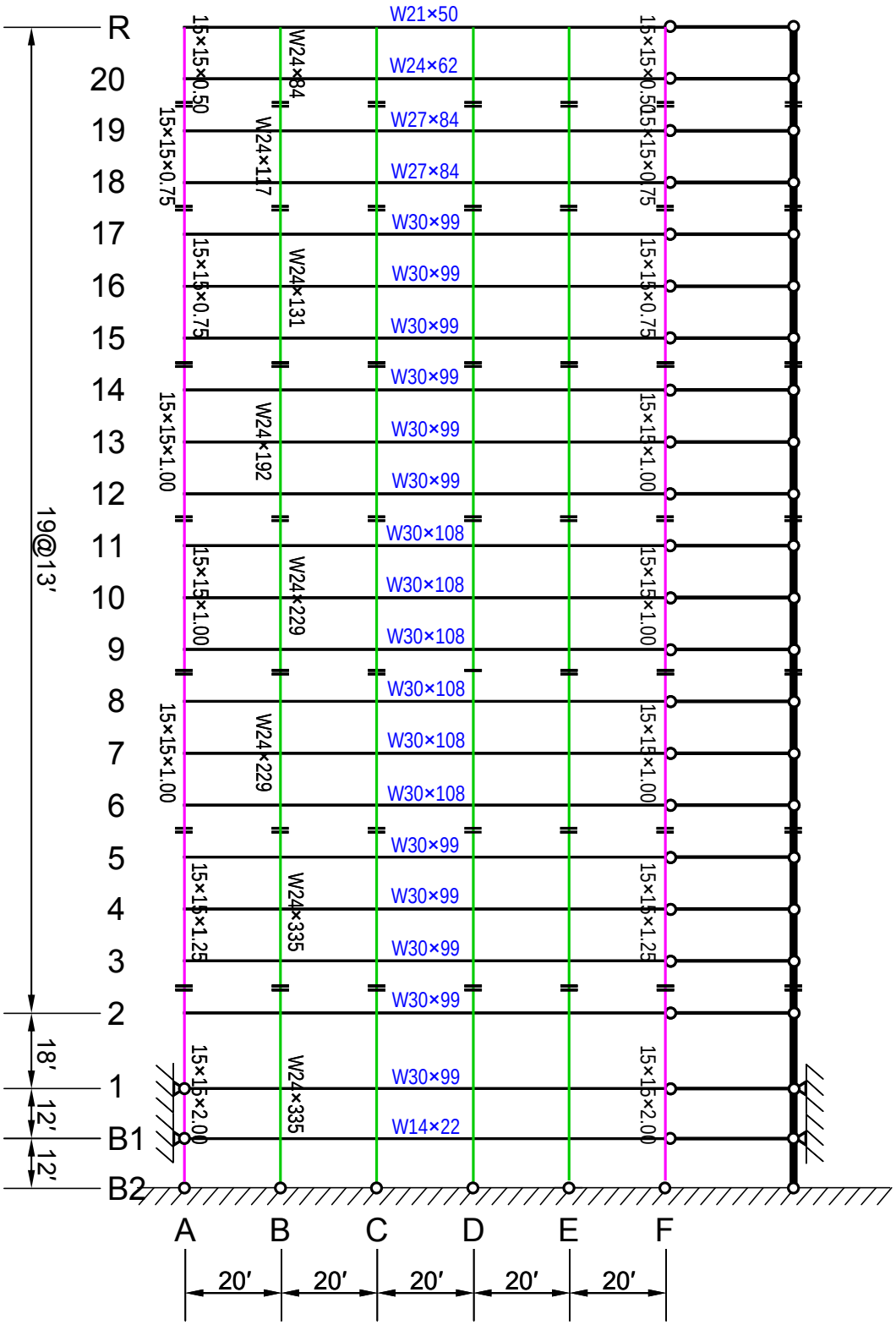

Figure A.3 – Los Angeles 20-Story Frame

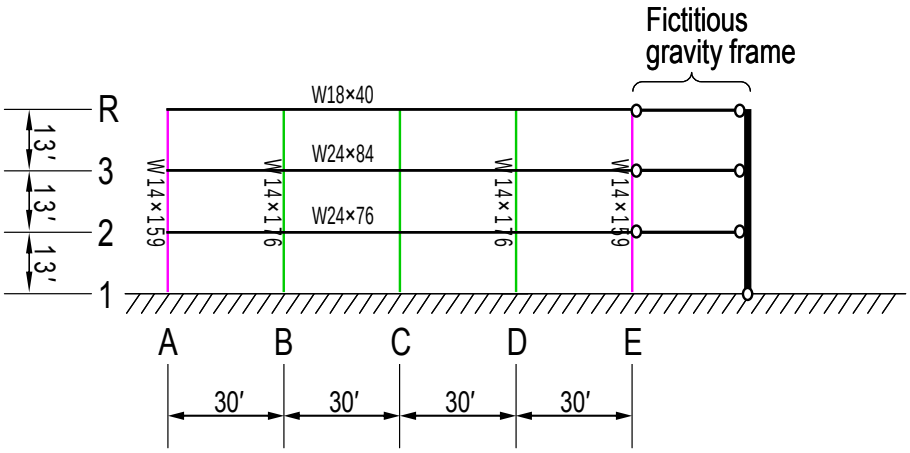

Figure A.4 - Seattle 3-Story Frame

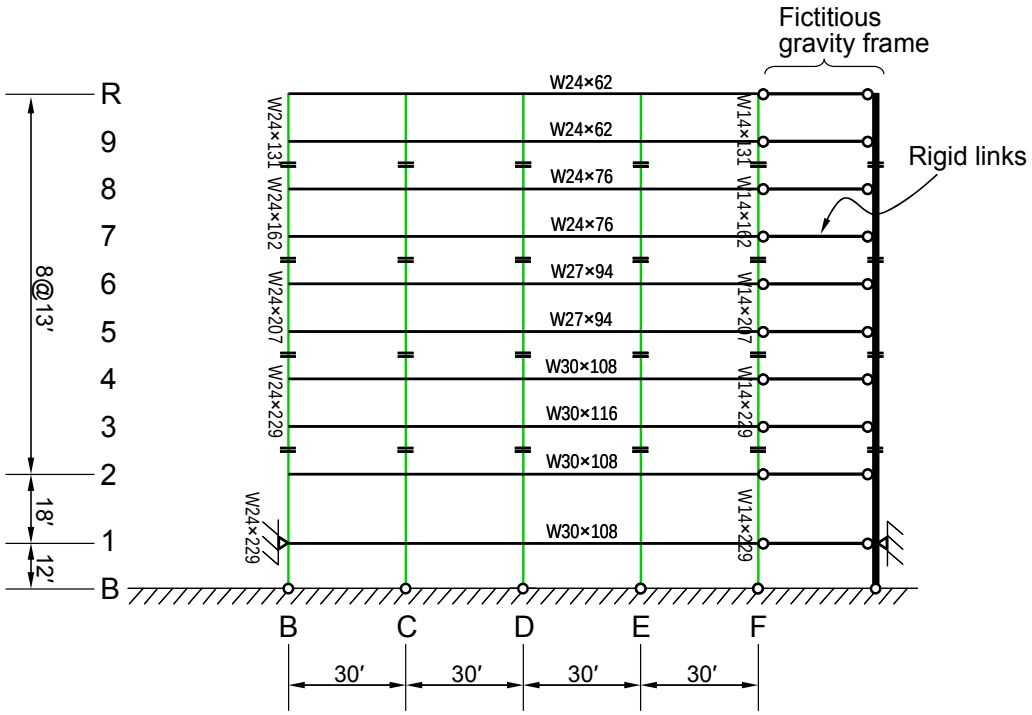

Figure A.5 - Seattle 9-Story Frame

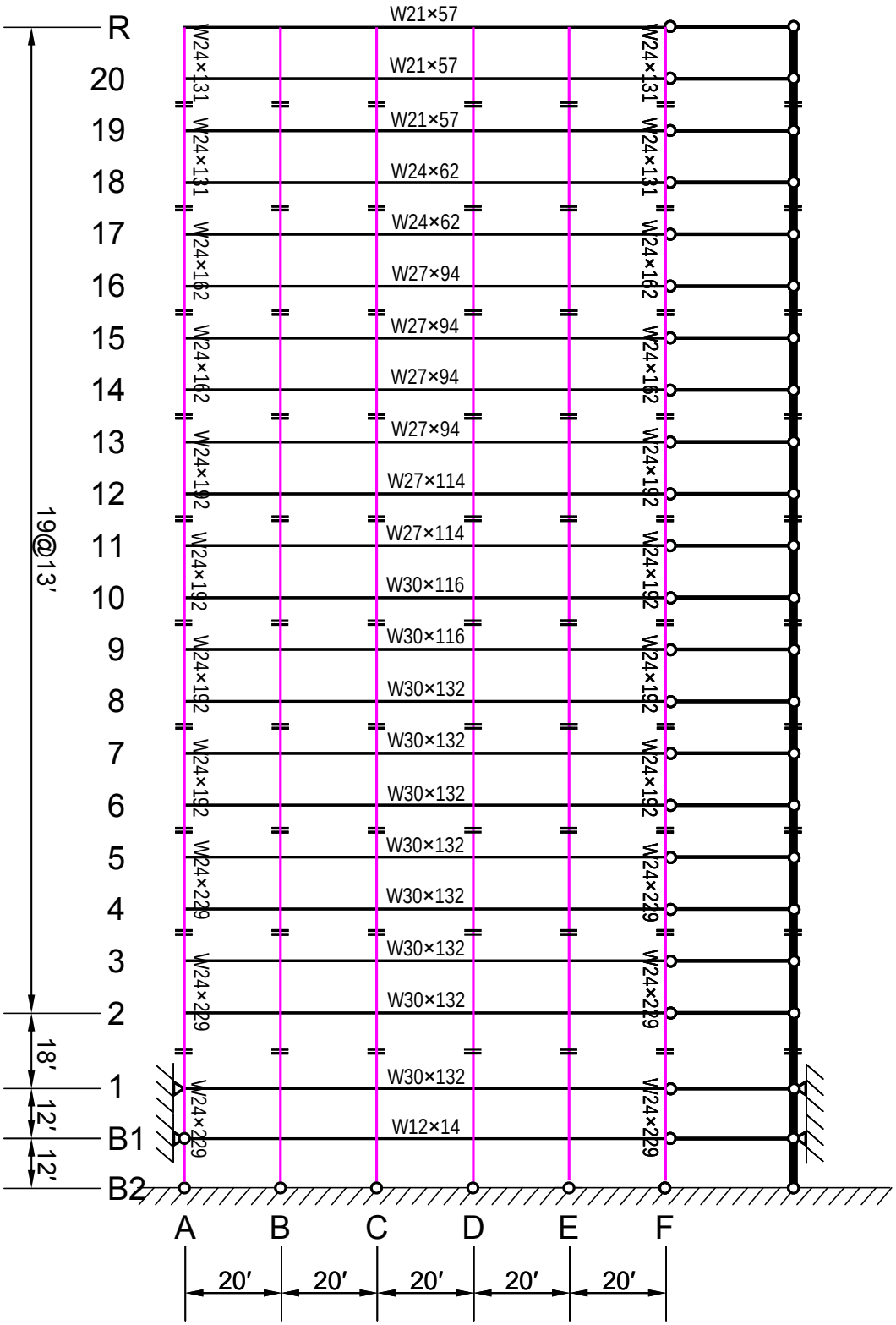

Figure A.6 - Seattle 20-Story Frame

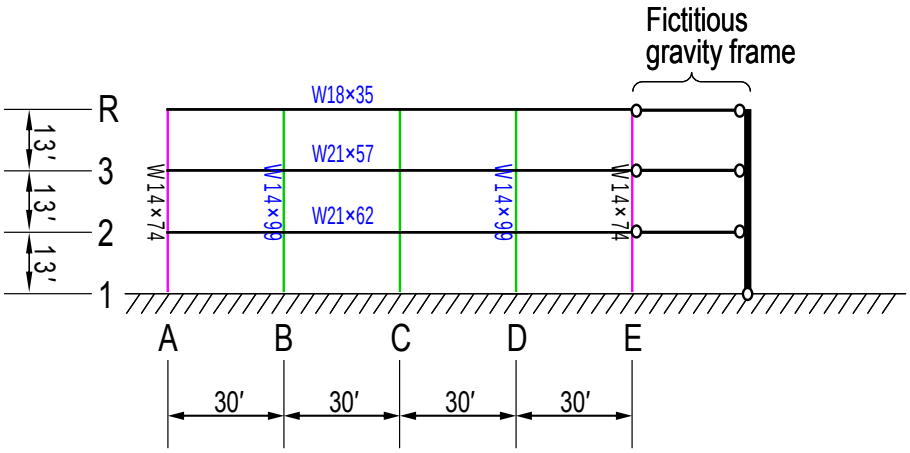

Figure A.7 - Boston 3-Story Frame

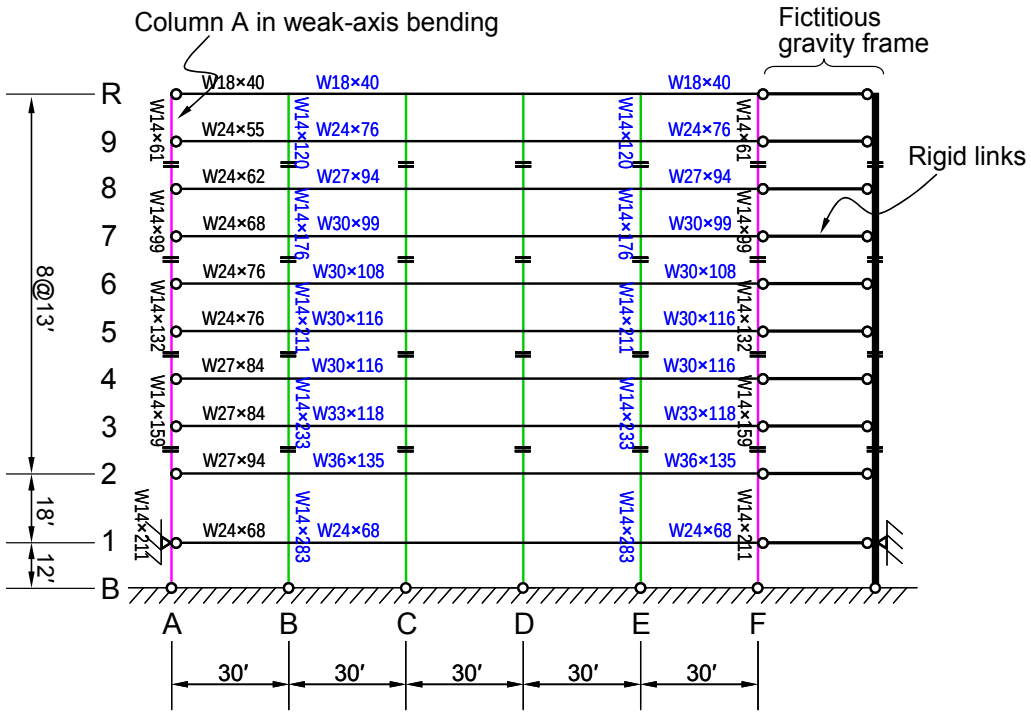

Figure A.8 - Boston 9-Story Frame

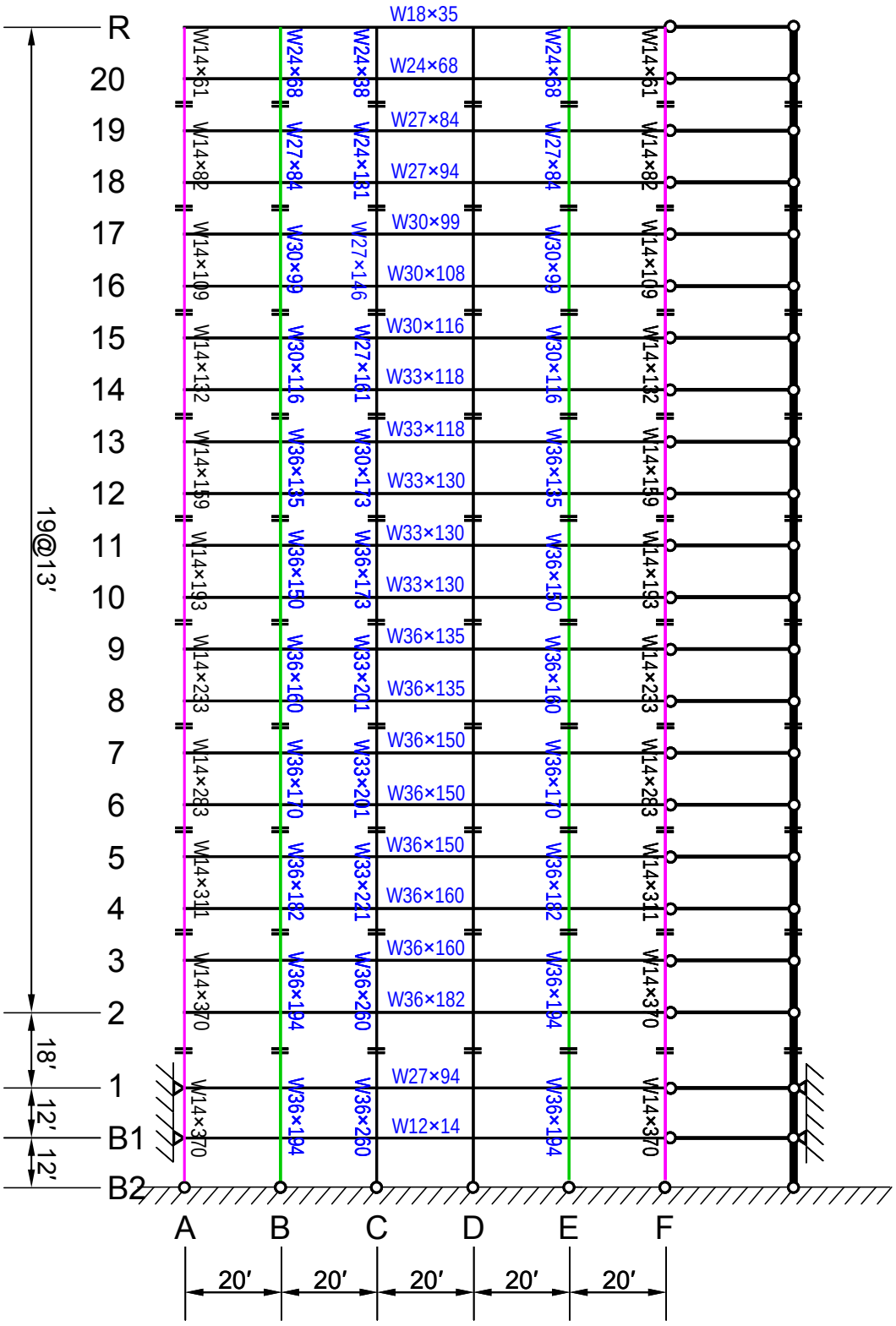

Figure A.9 - Boston 20-Story Frame

APPENDIX B

SPECTRAL CHARACTERISTICS OF SEISMIC INPUTS

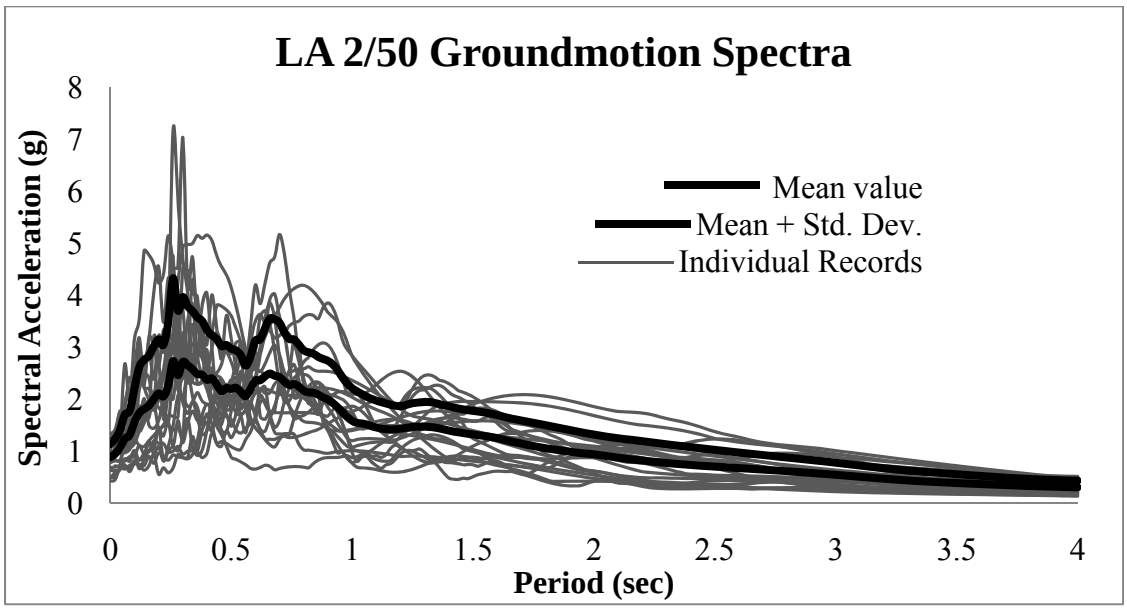

Figure B.1- Acceleration response spectra for LA 2/50 records with 2% damping

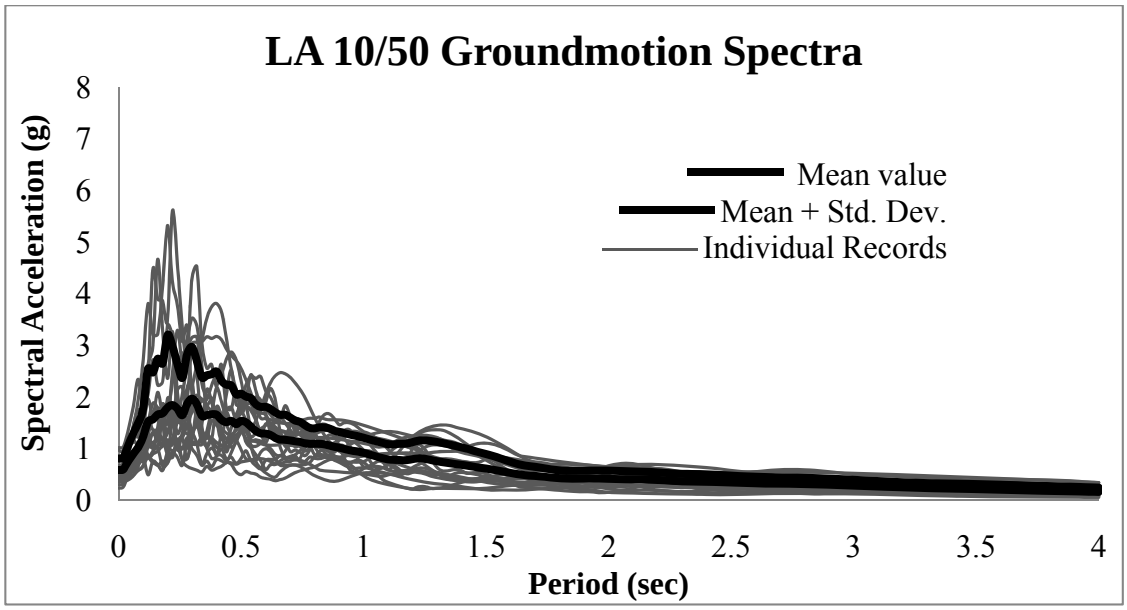

Figure B.2 - Acceleration response spectra for LA 10/50 records with 2% damping

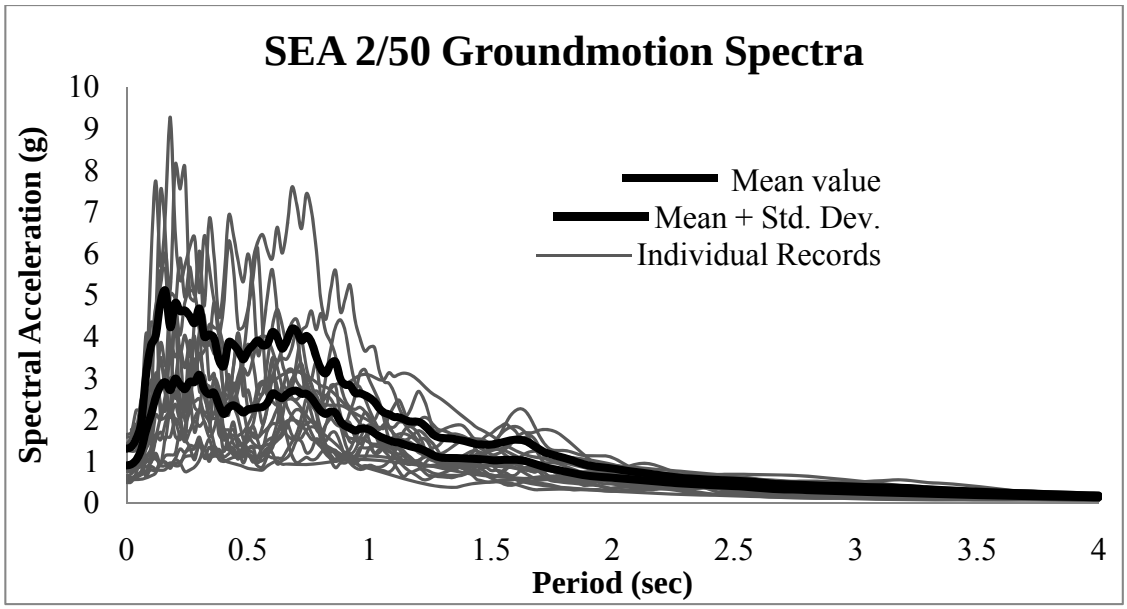

Figure B.3 - Acceleration response spectra for SEA 2/50 records with 2% damping

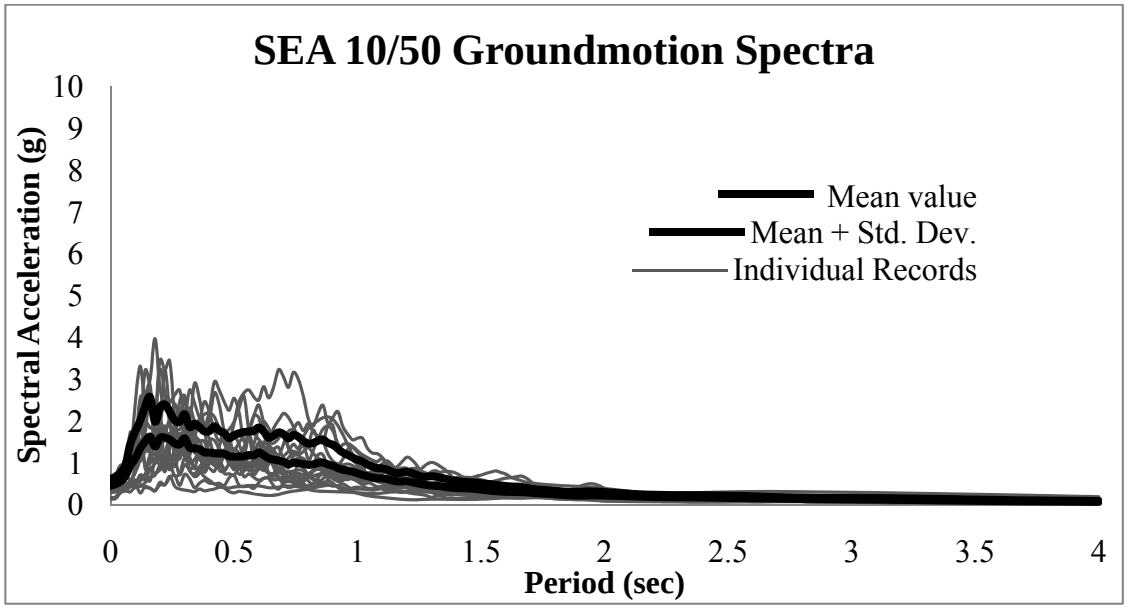

Figure B.4 - Acceleration response spectra for SEA 10/50 records with 2% damping

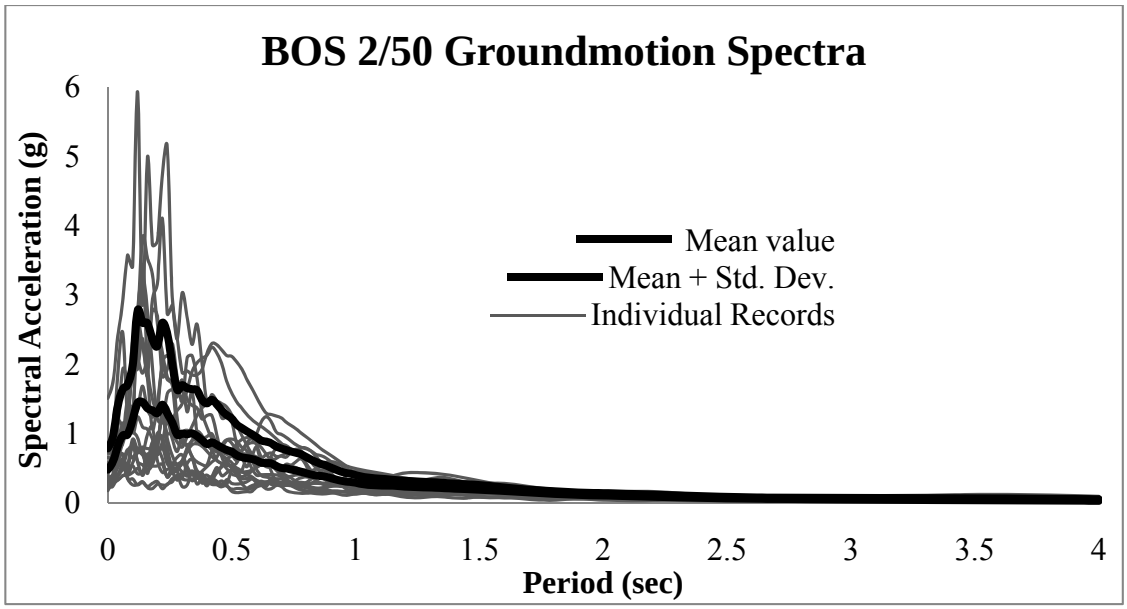

Figure B.5 - Acceleration response spectra for BOS 2/50 records with 2% damping

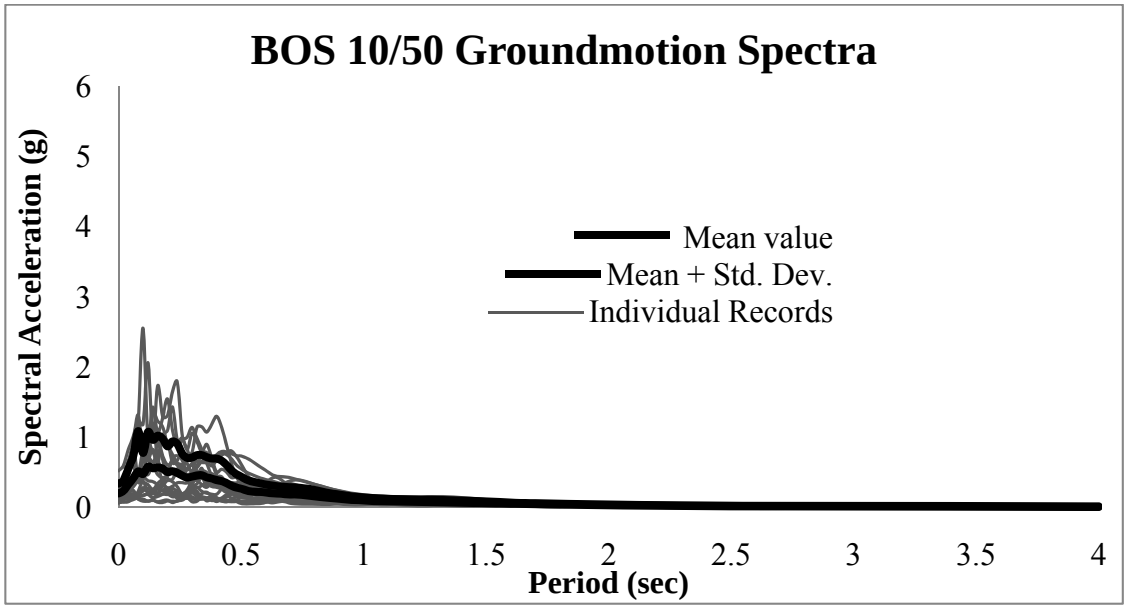

Figure B.6 - Acceleration response spectra for BOS 10/50 records with 2% damping

APPENDIX C
SEISMIC COLLAPSE BEHAVIOR OF BUILDINGS

C.1 Introduction

One of the primary objectives of research in structural earthquake engineering has been to understand, predict and prevent seismic collapse of buildings. Collapse is defined as the condition at which a structural system loses it's gravity-load carrying capacity, during a seismic excitation. Collapse may be local or global, where the former is said to have occurred when specific components undergo failure (e.g. buckling of some vertical load-carrying elements). Global collapse may have several causes, including ratcheting (drifting) of displacement response. Ratcheting generally occurs when the displacement demands in an earthquake are sufficiently severe to drive a structure into the range of negative post-yield lateral stiffness. Subsequently, the structure incrementally accumulates drift in a single direction. This may lead to sidesway (or incremental) collapse if an individual story (or a series of stories) displaces sufficiently so that second-order P-Δ effects fully offset the story shear resistance and the dynamic instability occurs i.e. the system loses its gravity load resistance.

The task of obtaining analytical predictions of dynamic instability for realistic buildings is an extremely complex one. This review discusses some of the attempts which have been made to predict and understand collapse behavior of structural systems.

C.2 Literature Review

One of the earliest studies on the role of P-Δ effects in seismic collapse was conducted by Jennings and Husid[1] (1968). They studied the behavior of a one-story frame with bilinear springs at the end of the columns, to account for material non-linearity. It was concluded that structural collapse can occur due to gravity loads acting through inelastic deformations that occur in response to ground shaking. Thus, such permanent deformations in the structure can lead to lateral instability and must be properly considered in modern design provisions

Takizawa and Jennings[2] (1980) used equivalent single-degree-of-freedom (SDOF) models to study the ultimate capacity of ductile reinforced concrete frame structures under the combined action of strong ground shaking and gravity loads. Their model exhibited a non-degrading tri-linear hysteretic behavior and explicitly accounted for P-Δ effects. They concluded that structural collapse is strongly influenced by the duration of ground motion and short-duration ground motions, in particular, have a low destructive capability, even if they have high peak ground accelerations. However, the latter conclusion was contradicted by findings of Hall et al.[3] (1995) and Krawinkler et al.[4] (2003).

---

[1] Jennings, P. C., and Husid, R. (1968). "Collapse of yielding structures during earthquakes." *Journal of Engineering Mechanics Division*, 94(5), 1045–1065

[2] Takizawa, H., and Jennings, P. C. (1980). "Collapse of a model for ductile reinforced concrete frames under extreme earthquake motions." *Earthquake Engineering and Structural Dynamics*, 8, 117–144

[3] Hall, J. F., Heaton, T. H., Halling, M. W., and Wald, D. J. (1995). "Near source ground motion and its effects on flexible buildings." *Earthquake Spectra*, EERI, 11(4), 569–605

[4] Krawinkler, H., Medina, R., and Alavi, B. (2003). "Seismic drift and ductility demands and their dependence on ground motions." *Engineering Structures*, 25(5), 637–653

Bernal[5,6] (1992,1998) employed equivalent SDOF models to compare dynamic failure modes with static failure mechanisms, predicted using mass proportional load distribution, and observed that the failure mode for a given building is either the same or varies little from one ground motion to another. Thus, a pushover analysis, using a lateral load distribution that is independent of the ground motion, may be a reasonable approach for identifying the critical mechanism.

Further, by studying two-dimensional moment-resisting frames Bernal concluded that: a) dynamic instability cannot be prevented by simply limiting the maximum elastic story drifts under design lateral loads; b) the intensity of ground motion required to induce instability is well correlated with the shape of the controlling failure mechanism (i.e. deformed configuration just before instability occurs). He also proposed a rational method to check the safety of two-dimensional buildings against dynamic instability. This method was based on ensuring that the base shear capacity of a building adequately exceeds an 'instability threshold' which, in turn, depends on the shape of the controlling failure mechanism for that building.

McRae[7] (1994) and Williamson[8] (2003) extended Bernal's studies to a more complex hysteretic response and both supported Bernal's conclusions, especially that the use of lateral drift as the only measure of damage, may not be appropriate in all cases. Williamson highlighted

---

[5] Bernal, D. (1992). "Instability of buildings subjected to earthquakes." *Journal of Structural Engineering*, ASCE, 118(8), 2239–2260

[6] Bernal, D. (1998). "Instability of buildings during seismic response." *Engineering Structures*, 20(4–6), 496–502

[7] MacRae, G. A. (1994). "*P*-Δ effects on single-degree-of-freedom structures in earthquakes." *Earthquake Spectra*, EERI, 10(3), 539–568

[8] Williamson, E. B. (2003). "Evaluation of damage and *P*-Δ effects for systems under earthquake excitation." *Journal of Structural Engineering*, ASCE, 129(8), 1036–1046

that in addition to P-Δ effects, rate of damage accumulation also contributes significantly to the computed response of a model structure. Thus, there is a need to use models that explicitly consider the level of damage in determining seismic response of a system.

Challa and Hall[9] (1994) investigated the collapse capacity of a 20-story steel moment-resisting frame. They observed significant plastic hinging in the columns and a high potential for collapse under severe ground motion. This was despite the fact that the frame was designed using the 'strong-column weak-beam' philosophy emphasized in modern seismic design provisions. Their findings were recently corroborated by Medina and Krawinkler[10] (2005) who investigated the possibility of brittle failure modes in columns of moment-resisting steel frames, to provide guidance for improvement of current design provisions. They evaluated both local and global strength demands using nonlinear dynamic analysis and compared the results with those from nonlinear static analysis. It was observed that dynamic base shear demand and distribution of story forces can be significantly different from values obtained using static analysis. Moreover, due to effects of higher modes (particularly the second mode) and inelastic redistribution of forces, the point of inflection in a column can move from mid-height to one of the column ends, thereby producing a condition of single curvature in the column. Thus, there exists a potential for plastic hinging in columns designed using current provisions and more stringent strong-column/weak-beam criteria may be needed.

---

[9] Challa, V. R. M., and Hall, J. F. (1994). "Earthquake collapse analysis of steel frames." *Earthquake Engineering and Structural Dynamics*, 23(11), 1199–1218

[10] Medina, R. A., and Krawinkler, H. (2005). "Strength design issues relevant for the seismic design of moment-resisting frames." *Earthquake Spectra*, EERI, 21(2), 415–439

Roeder et al.[11] (1993) studied an eight-story steel moment-resisting frame designed according to the minimum design criteria of 1988 *Uniform Building Code* (UBC). They found that UBC methods for limiting drift and requiring a minimum seismic design force are not adequate to ensure that the inelastic story drifts of a structure are always below the maximum values considered in its design. Better performance can be achieved, particularly for shorter structures, if the drift limits are checked with the same seismic forces as are used in the strength design. However, this issue has still not been addressed in the latest version of *ASCE-7*.

A study by Martin and Villaverde[12] (1996) further raised questions about modern design provisions when they observed that a two-story, two-bay steel moment-resisting frame collapsed under a moderately strong ground motion even when the structure met all the requirements of the 1992 AISC *Seismic Provisions*[13].

Following the Northridge earthquake in 1994, the FEMA-SAC Steel Project[14] was initiated with the goal of investigating damage to welded steel moment-resisting frame buildings and developing repair techniques and new design approaches to minimize such damage in future earthquakes. Lee and Foutch[15,16,17] (2002a,b and 2006) conducted a series of analytical studies

---

[11] Roeder, C. W., Schneider, S. P., and Carpenter, J. E. (1993). "Seismic behavior of moment-resisting steel frames: Analytical study." *Journal of Structural Engineering*, ASCE, 119(6), 1866–1884

[12] Martin, S. C., and Villaverde, R. (1996). "Seismic collapse of steel frame structures." *Proceedings, 11th World Conference on Earthquake Engineering*, Acapulco, Mexico, Paper No. 475

[13] American Institute of Steel Construction. (1992). *Seismic Provisions for Structural Steel Buildings*. ANSI/AISC Standard 341. AISC, Chicago, Illinois.

[14] Federal Emergency Management Agency (2000). *State of the Art Report on Systems Performance of Steel Moment Resisting Frames Subject to Earthquake Ground Shaking*, FEMA 355C.

[15] Lee, K., and Foutch, D. A. (2002a). "Performance evaluation of new steel frame buildings for seismic loads." *Earthquake Engineering and Structural Dynamics*, 31(3), 653–670

[16] Lee, K., and Foutch, D. A. (2002b). "Seismic performance evaluation of pre-Northridge steel frame buildings with brittle connections." *Journal of Structural Engineering*, ASCE, 128(4), 546–555

for performance prediction of existing pre-Northridge buildings, comparison with Post-Northridge buildings and evaluation of modern seismic design provisions. In all of these studies, the basic methodology adopted by Lee and Foutch was to: a) evaluate *seismic drift capacity* (maximum story drift) of the building model using Incremental Dynamic Analysis b) find statistical *drift demands* (median, 84th and 95th percentile) using nonlinear dynamic analysis for 20 ground motions representing 2/50 and 50/50 hazard levels c) finally, calculate *confidence level* for Collapse Prevention (CP) or Immediate Occupancy (IO) performance objectives by using Demand to Capacity Ratio (DCR) and other numerical factors to account for uncertainty involved in the analyses.

Lee and Foutch observed that all post-Northridge buildings, designed according to the 1997 NEHRP[18] guidelines, showed a high confidence level (>90%) of satisfying CP or IO performance objectives. However, as expected, pre-Northridge buildings exhibited a much lower confidence level. Moreover, in order to evaluate the effect of R-factor (strength reduction factor), they conducted dynamic analysis of 3-, 9- and 20-story buildings designed with R-values varying from 8 to 12. The effect of provision for lower bound on design response spectrum (C_s) was also investigated. It was concluded that current provisions (R = 8 and lower-bound on C_s) lead to conservative designs which could provide good protection against dynamic instability during earthquakes. Further, the lower-bound on C_s should not be dropped from newer versions of *ASCE-7*.

---

[17] Lee, K., and Foutch, D. A. (2006). "Seismic evaluation of steel moment frame buildings designed using different R-values." *Journal of Structural Engineering*, ASCE, 132(9), 1461-1472

[18] Federal Emergency Management Agency (1998). *NEHRP Recommended Provisions for Seismic Regulations for New Buildings and Other Structures, Part 1—Provisions, 1997 Edition*. FEMA 302, Washington DC.

In an attempt to improve the current understanding of structural collapse, Ibarra and Krawinkler[19] (2005) proposed a collapse assessment methodology that takes into account both the P-Δ effect and stiffness and strength deterioration of structural components. For this purpose, they developed a hysteretic model which was capable of capturing basic strength as well as cyclic deterioration based on rules proposed by Rahnama and Krawinkler[20] (1993). Next, they calibrated this model utilizing experimental data from tests of steel, plywood, and reinforced concrete components and then employed these models to calculate collapse capacities of SDOF systems and MDOF frame structures. They identified parameters that mostly influence collapse and assessed the sensitivity of collapse capacity to these parameters. It was concluded that deterioration is an overriding consideration in the seismic response analysis of a structure when the structure is near the limit state of collapse.

This work has been further extended by Lignos[21] (2008). In his study, Lignos has modified the Ibarra-Krawinkler model to better approximate the observed experimental behavior of steel components deteriorating in a local or lateral torsional buckling mode. Another major outcome of this work has been the creation of a large database in which the modified Ibarra-Krawinkler model was calibrated against experimental results from hundreds of steel wide-flange beams and columns, steel tubular sections and RC beams and columns. Using this statistical information, empirical equations were proposed that associate deterioration modeling

---

[19] Ibarra, L. F., Medina, R. A., and Krawinkler, H. (2005). "Hysteretic models that incorporate strength and stiffness deterioration." *Earthquake Engineering and Structural Dynamics*, 34(12), 1489–1511

[20] Rahnama, M. and Krawinkler, H. (1993). "Effect of soft soils and hysteresis models on seismic design spectra," *John A. Blume Earthquake Engineering Research Center* Report No. 108, Department of Civil Engineering, Stanford University

[21] Lignos, D. (2008). "Sidesway collapse of deteriorating structural systems under seismic excitations." *PhD. Thesis,* Stanford University, Stanford, CA.

parameters with geometric and material properties of beams and columns. Finally, experimental and analytical case studies were conducted and a good correlation was observed between analytical predictions and experimental results. Thus, it was concluded that it is possible to predict collapse capacity of structures, with a satisfactory level of accuracy, provided that the deterioration characteristics of critical components are adequately represented in the analytical models. Studies by other researchers, like Ayoub et al.[22] (2004), are also noteworthy in this context.

Villaverde[23] (2007) presents an excellent discussion of methodologies that are currently available to assess collapse capacities of structures under earthquake ground motions. By reviewing several analytical studies, accuracy and limitations of the following are presented: a) SDOF models b) Nonlinear Static Procedure c) Step-by-Step Finite Element Analyses d) Incremental Dynamic Analyses. Villaverde concludes that currently available methods are not entirely satisfactory and there is a need for reliable experimental studies on collapse behavior, to verify analytical results.

More recently, researchers have focused their attention to developing relations between a ground motion intensity measure (IM) and the probability of collapse, denoted as *collapse fragility curve*, and the relation between the same ground motion IM and the seismic hazard for the building, denoted as *seismic hazard curve*. In this context, Zareian et al.[24] (2009) present two

---

[22] Ayoub, A., Mijo, C., and Chenouda, M. (2004). "Seismic fragility analysis of degrading structural systems." *Proceedings, 13th World Conference on Earthquake Engineering*, Vancouver, B.C., Canada, Paper No. 2617

[23] Villaverde, R. (2007). "Methods to assess seismic collapse capacity of structure: state of the art." *Journal of Structural Engineering*, ASCE, 133(1), 57–66

[24] Zareian, F., Krawinkler, H., Ibarra, L., and Lignos, D. (2009). "Basic concepts and performance measures in prediction of collapse of buildings under earthquake ground motions." *Structural Design of Tall and Special Buildings*, 19(1), 167–181

approaches for estimating the collapse fragility curve of a building, both utilizing Incremental Dynamic Analysis. Limitations of these methods, along with scope for future work, have also been discussed.

APPENDIX D

CALCULATION OF DESIGN BASE SHEAR FOR INTERACTION CHECKS FOR LA-9

D.1 Design base shear per *ASCE-7*:

Response modification factor: $R = 8$ (assuming special moment-resisting frame)

Response modification factor: $I = 1.0$ (for Occupancy category II)

Fundamental period: $T_a = C_t \cdot (h_n)^x = 0.028 \times 122^{0.8} = 1.31$ (sec)

or $T_a = 0.1N = 0.1 \times 9 = 0.9$ (sec)

and T_b (found from Eigen value analysis) = 2.26 sec

per *ASCE-7* 12.8.2: $T \le C_u T_a = 1.4 \times 1.31 = 1.83 \,\text{sec}$

$\Rightarrow T = 1.83 \,\text{sec}$

Spectral acceleration:	$S_S = 2.43g$	$S_1 = 0.85g$
Site Class D (stiff soil)	$F_a = 1.0$	$F_v = 1.5$
Spectral acceleration for MCE:	$S_{MS} = F_a S_S = 2.43g$	$S_{M1} = F_v S_1 = 1.28g$
Design spectral acceleration:	$S_{DS} = 2/3 \times S_{MS} = 1.62g$	$S_{D1} = 2/3 \times S_{M1} = 0.85g$

Design response spectrum: $T_0 = 0.2\, S_{D1} / S_{DS} = 0.105$ (sec)

$T_S = S_{D1} / S_{DS} = 0.525$ (sec)

$T_L = 6$ sec

Fit to Table A.1 in *ASCE-7*

$$T_L = 8 \text{ sec}$$

$$C_s = \frac{S_{DS}}{\frac{R}{I}} = \frac{1.62}{\frac{8}{1}} = 0.2025 \leq \left\{ \frac{S_{D1}}{T(\frac{R}{I})} = \frac{0.85}{1.83(\frac{8}{1})} = 0.0581 \right\} \quad \rightarrow \boldsymbol{C_s = 0.058}$$

Check: $C_s = 0.058 > 0.01$ → OK

$$\text{and } \because S_1 > 0.6(g) \Rightarrow C_s > \left\{ \frac{0.5S_1}{\frac{R}{I}} = \frac{0.5 * 0.85}{\frac{8}{1}} = 0.053 \right\} \rightarrow \text{OK}$$

C_s = 0.058

D.2 <u>Design base shear per *Uniform Building Code* (UBC) 1994</u>

As per UBC ’94:

$$V_s = \left(\frac{ZIC}{R_w} \right) W$$

Where

Z = Seismic Zone Factor = 0.4 (for Zone 4 i.e LA)

I = Importance Factor = 1.0 (office building)

$$C = \frac{1.25S}{T^{2/3}} \leq 2.75$$

S = Site Coefficient = 1.2 (for stiff soil)

$T_a = C_t(h)^{0.75} = 0.035 \times 122^{0.75} = 1.28\,\text{sec}$; $T_b = 2.26\,\text{sec}$ (Eigen value analysis)

per UBC '94: $T \le C_u T_a = 1.3 \times 1.28 = 1.66\,\text{sec}$

$\Rightarrow T = 1.66\,\text{sec}$

$$\Rightarrow C = \frac{1.25 \times 1.2}{1.66^{2/3}} = 1.07$$

R_w = Response Modification for SMRFs per Allowable Stress Design (ASD) approach = 12

$$\Rightarrow C_s = \frac{0.4 \times 1.0 \times 1.07}{12} = 0.0357 \text{ (base-shear coefficient for ASD)}$$

But since our purpose is to conduct LRFD design checks, the difference between ASD and LRFD approaches must be accounted for in two ways:

1) The difference between R_w and R needs to be taken into consideration
2) ASD allows a 33% increase in allowable stress for seismic design. This also needs to be accounted for.

$$\therefore (C_s)_{LRFD} = (C_s)_{ASD} \times \frac{1}{1.33} \times \frac{R_w}{R} = 0.0357 \times \frac{1}{1.33} \times \frac{12}{8} = 0.0403$$

Thus, a representative value of C_s for conducting design interaction checks:

C_s = 0.04 *(less than the value prescribed by ASCE-7)*